RESEARCH ARTICLE

Melt pond CO₂ dynamics and fluxes with the atmosphere in the central Arctic Ocean during the summer-to-autumn transition

Masaki Yoshimura[1],* [iD], Daiki Nomura[1,2,3], Alison L. Webb[4,5], Yuhong Li[6], Manuel Dall'osto[7], Katrin Schmidt[8], Elise S. Droste[9,10], Emelia J. Chamberlain[11,12], Kevin M. Posman[13], Hélène Angot[14], Byron Blomquist[15,16], Hanno Meyer[17], Mario Hoppema[9], Manami Tozawa[1], Jun Inoue[18], and Bruno Delille[19]

Melt ponds are a common feature of the Arctic sea-ice environment during summer, and they play an important role in the exchange of heat and water vapor between the ocean and the atmosphere. We report the results of a time-series study of the CO_2 dynamics within melt ponds (and nearby lead) and related fluxes with the atmosphere during the summer-to-autumn transition in the central Arctic Ocean during the Multidisciplinary drifting Observatory for the Study of Arctic Climate (MOSAiC) expedition. In late summer 2020, low-salinity meltwater was distributed throughout the melt ponds, and undersaturation of pCO_2 in the meltwater drove a net influx of CO_2 from the atmosphere. The meltwater layer subsequently thinned due to seawater influx, and a strong gradient in salinity and low-pCO_2 water was observed at the interface between meltwater and seawater at the beginning of September. Mixing between meltwater and underlying seawater drives a significant drawdown of pCO_2 as a result of the non-linearities in carbonate chemistry. By the middle of September, the strong stratification within the meltwater had dissipated. Subsequent freezing then began, and cooling and wind-induced drifting of ice floes caused mixing and an influx of seawater through the bottom of the melt pond. The pCO_2 in the melt pond reached 300 μatm as a result of exchanging melt pond water with the underlying seawater. However, gas exchange was impeded by the formation of impermeable freshwater ice on the surface of the melt pond, and the net flux of CO_2 was nearly zero into the pond, which was no longer a sink for atmospheric CO_2. Overall, the melt ponds in this Arctic sea-ice area (both melt ponds and lead water) act as moderate sinks for atmospheric CO_2.

Keywords: Carbon dioxide, Melt ponds, Sea ice, Carbonate chemistry, Arctic Ocean

1. Introduction

The Arctic is predicted to be affected more strongly by global warming than other regions, with temperatures rising about four times faster than the global average (Ono et al., 2022; Rantanen et al., 2022). Along with rising air temperatures, the extent of Arctic sea ice has been

[1] Faculty/Graduate School of Fisheries Sciences, Hokkaido University, Sapporo, Hokkaido, Japan

[2] Field Science Center for Northern Biosphere, Hokkaido University, Sapporo, Hokkaido, Japan

[3] Arctic Research Center, Hokkaido University, Sapporo, Hokkaido, Japan

[4] School of Life Sciences, University of Warwick, Coventry, UK

[5] Current address: Wolfson Atmospheric Chemistry Laboratories, University of York, York, UK

[6] Third Institute of Oceanography, Ministry of Natural Resources, Xiamen, China

[7] Institute of Marine Science, Consejo Superior de Investigaciones Científicas (CSIC), Barcelona, Spain

[8] School of Geography, Earth and Environmental Sciences, University of Plymouth, Plymouth, UK

[9] Alfred Wegener Institute Helmholtz Centre for Polar and Marine Research, Bremerhaven, Germany

[10] School of Environmental Sciences, University of East Anglia, Norwich, UK

[11] Scripps Institution of Oceanography, University of California San Diego, La Jolla, USA

[12] Woods Hole Oceanographic Institution, Woods Hole, MA, USA

[13] Bigelow Laboratory for Ocean Sciences, Boothbay, ME, USA

[14] Univ. Grenoble Alpes, CNRS, INRAE, IRD, Grenoble INP, IGE, Grenoble, France

[15] National Oceanic and Atmospheric Administration (NOAA) Physical Sciences Laboratory (PSL), Boulder, CO, USA

[16] Cooperative Institute for Research in Environmental Sciences (CIRES), University of Colorado, Boulder, CO, USA

[17] Alfred Wegener Institute Helmholtz Centre for Polar and Marine Research, Potsdam, Germany

[18] National Institute of Polar Research, Tachikawa, Japan

[19] Unité d'Océanographie Chimique, Freshwater and Oceanic Science Unit of Research (FOCUS), Université de Liège, Liège, Belgium

* Corresponding author:
Email: masaki.yoshimura@eis.hokudai.ac.jp

decreasing (Polyakov et al., 2012; Stroeve et al., 2012); the lowest extent of sea ice in recorded history was reported in 2012 (National Snow and Ice Data Center, 2024). There are many impacts of the reduction of the extent of sea ice. For example, ocean circulation changes due to alteration of the density structure caused by increased meltwater flow into the oceanic surface layer.

The Arctic Ocean and its adjacent seas north of 60°N show high solubility of CO_2 due to the low water temperatures in the Arctic (Bates et al., 2006), absorbing 180 $\pm$ 130 Tg C yr^{-1} from the atmosphere, which is 5% to 14% of the total CO_2 absorption by the global ocean (Bates and Mathis, 2009; Takahashi et al., 2009; Yasunaka et al., 2018). In the region where sea ice occurs, the increased solar radiation and air temperatures during the summer promote the melting of snow and sea ice, with the meltwater entering the ocean surface layer as freshwater (Smith et al., 2023). Meltwater from sea ice and snow can enter the ocean surface layer from the edges and bottoms of sea ice, or it can flow through cracks or leads in the sea ice (Eicken, 1994; Richter-Menge et al., 2001; Eicken et al., 2002; Nomura et al., 2018a; 2023). In addition, meltwater accumulates in depressions on the sea-ice surface, forming melt ponds. The seasonal evolutionary process of melt ponds can be divided into four stages (Eicken et al., 2002). In the first stage, snow on sea ice melts and accumulates on the surface of the sea ice. The sea ice at this time has low permeability, so the meltwater does not percolate through the sea ice, but spreads horizontally and drains into cracks, leads, or seal holes and reaches the ocean surface. In the second stage, most of the snow has melted, and the melt pond area (melt pond fraction) increases and approaches a maximum. However, the size of the melt ponds will start to decrease because of horizontal transport and an increase in the number of downward meltwater runoff pathways due to increased sea-ice permeability. Melt ponds also drain due to the increased hydrostatic pressure when too much water is accumulated above freeboard, the sea-ice floating line (Polashenski et al., 2012). In the third stage, further increases in the permeability of the sea ice result in more downward drainage. In addition, meltwater is less likely to be retained on the sea-ice surface as the sea ice breaks up. In many cases, however, the fraction of melt pond area to sea-ice area may reach a maximum at this stage because the elevation of the sea-ice surface becomes lower than the freeboard as the sea ice thins, and new melt ponds are then formed from surface flooding or underlying seawater intrusion (Polashenski et al., 2012). If melt ponds persist through the summer into the winter, then they refreeze and, after snow accumulates on their surfaces, are no longer visible. This is the fourth stage of melt ponds (Eicken et al., 2002; Petrich et al., 2012; Smith et al., 2023).

Melt ponds are a common and natural feature of the Arctic sea-ice environment during summer. The presence of melt ponds accelerates sea-ice melting by reducing the albedo of the area where sea ice is present, thereby warming the upper ocean (Curry et al., 1995; Perovich et al., 2002; Eicken et al., 2004). Melt ponds are categorized as "open ponds" or "closed ponds" depending on whether they are connected to seawater or not (Eicken et al., 2004; Lee et al., 2012). Melt ponds have been found to harbor both freshwater and saltwater phytoplankton and bacteria (Melnikov et al., 2002; Gradinger et al., 2005; Nomura et al., 2011; Fernández-Méndez et al., 2014; 2015; Sørensen et al., 2017). They also temporarily trap atmospheric trace elements that have accumulated within the snow, and release them into the surface ocean after photochemical reactions (Marsay et al., 2018). A melt pond is thus a transitional environment with various physical, chemical, and biological impacts in the region of Arctic sea ice.

Studies of melt ponds have used satellites to determine the ratio of melt pond area to sea-ice surface area (Rösel and Kaleschke, 2011; Webster et al., 2022) and modeling to investigate melt pond geometry and physical processes (e.g., Taylor and Feltham, 2004; Polashenski et al., 2012). Those studies have revealed that melt ponds cover about 20−50% of the area of summer Arctic sea ice (Polashenski et al., 2012; Feng et al., 2022; Webster et al., 2022). Despite such widespread coverage, relatively few studies have been conducted to constrain the CO_2 budget in melt ponds (Semiletov et al., 2004; Bates et al., 2014; Geilfus et al., 2015), and all were conducted in areas of first-year sea ice in coastal areas of Alaska and the Canadian Arctic. Semiletov et al. (2004) and Geilfus et al. (2015) found that melt ponds absorb CO_2 from the atmosphere (-5.4 to -0.0 mmol m^{-2} day^{-1}; negative values indicate CO_2 absorption from the atmosphere) by having lower pCO_2 in melt ponds on Arctic sea ice than in the atmosphere.

A long-term drifting observational study broken up into 5 consecutive legs—Multidisciplinary drifting Observatory for the Study of Arctic Climate (MOSAiC)—was conducted in the central Arctic Ocean from October 2019 to September 2020 (Nicolaus et al., 2022; Shupe et al., 2022). We collected various data over a year in the region of central Arctic sea ice, where year-round observations are difficult to make. During that study, our observations took place during Leg 5 (August to October 2020) when melt ponds had matured (late summer) to the time when the surface of the melt ponds froze in early autumn. There have been no reports of melt pond carbonate chemistry in multi-year ice areas of the central Arctic Ocean. Nor have any studies examined in detail the vertical profiles of biogeochemical components inside melt ponds, the relationship between the structure of the melt pond interior and CO_2 dynamics, and the impact on the flux of CO_2 between the atmosphere and sea ice. The objectives of this study were to (1) describe the relationship between the physical environment and CO_2 dynamics inside the melt ponds, (2) evaluate the effect of mixing of meltwater and seawater inside the melt ponds on carbonate chemistry, and (3) describe the process of CO_2 exchange between the melt ponds and the atmosphere. The resulting data will enable future predictions of the effects of further sea-ice melting and meltwater inflow on the Arctic Ocean carbonate chemistry and fluxes between the atmosphere and the Arctic Ocean.

2. Materials and methods

2.1. Observation date and site

Surveys of melt ponds on sea ice and nearby leads were carried out during MOSAiC Leg 5 (August 22 to September 24, 2020) in the multi-year pack ice region of the central Arctic Ocean on board the R/V *Polarstern* (**Figure 1**). During Leg 4, the vessel drifted to the ice edge in Fram Strait and was thereafter relocated to the central Arctic Ocean to study the onset and early freezing phase of the sea ice.

On the initial arrival at the Leg 5 floe, multi-year ice with a thickness of 1.6 m based on measurements at the ice-coring site (**Figure 1**), a survey of 12 melt ponds was undertaken, selected to cover a broad range of sizes and shape (**Table 1**; **Figure 1**). After the breakup of the floe at the beginning of the survey (August 24), several of the melt ponds were inaccessible, and two of the melt ponds had been destroyed by a crack that opened directly through them (Stations 3 and 8, which were observed as
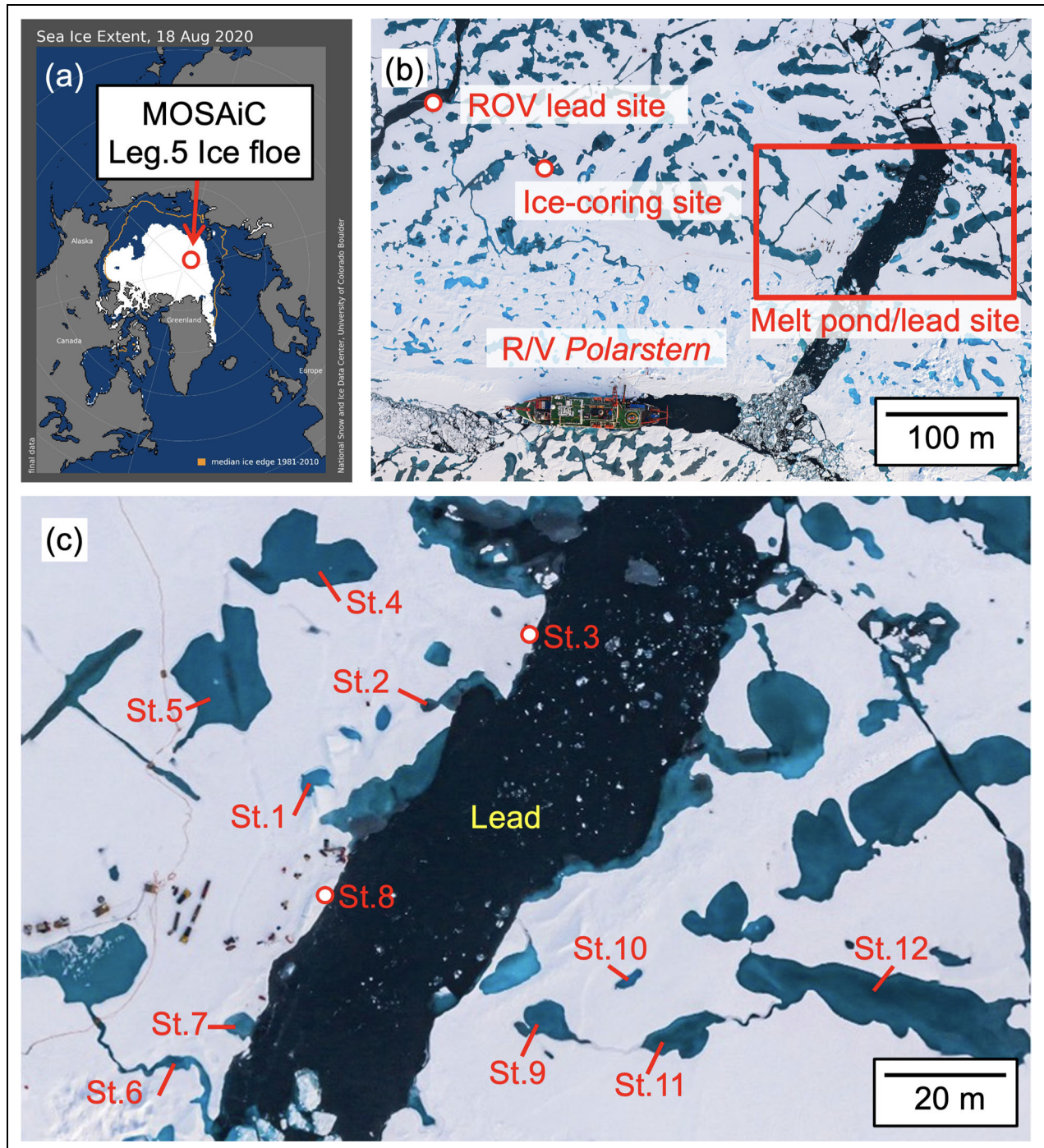

Figure 1. MOSAiC Leg 5 study area in the central Arctic Ocean. (a) Location of MOSAiC Leg 5 in the central Arctic Ocean. (b) Map of the sampling locations on the MOSAiC Leg 5 ice floe. This image was obtained on August 25, 2020, by a drone (operated by S Graupner). (c) Enlargement of the red box in (b) to show sampling stations (St.) in melt ponds and the lead.

Table 1. Melt pond station, type (open or closed), size, temperature, salinity, dissolved inorganic carbon (DIC), total alkalinity (TA), and pCO$_2$ on August 22, 2020

Station (Type)[a]	Pond, Size (m^2)[b]	Sampling Depth (m)	Temperature (°C)	Salinity	DIC (μmol kg^{-1})	TA (μmol kg^{-1})	pCO$_2$ (μatm)
1 (closed)	17	0.3[c]	0.5	0.8	73	63	138
2 (open)	5	0.3	0.1	1.1	102	79	296
3 (open)	(crack)	0.3	0.1	1.8	143	125	246
4 (open)	192	0.3[d]	0.2	0.2	45	16	370
5 (open)	233	0.3	0.1	0.2	44	15	364
6 (closed)	14	0.3	0.1	0.3	50	20	386
7 (closed)	23	0.3	0.0	0.3	56	28	363
8 (open)	(crack)	0.3	0.0	0.6	66	42	309
9 (closed)	48	0.3	0.2	2.3	179	159	277
10 (closed)	8	0.3	0.1	0.3	60	36	308
11 (open)	63	0.3	0.6	2.2	162	141	279
12 (open)	444	0.3	0.1	1.4	124	97	362
Average		0.3	0.7	1.0	94	71	314
Standard deviation			±0.5	±0.8	±48	±51	±74

[a]An additional station was established at the ice-coring site (**Figure 1**) after development of an open pond of 356 m^2.

[b]Depth of the melt pond at Station 1 was 0.3 m; at Station 4, the depth range was 0.5–1.2 m over the study period, August 23–September 14, 2020.

[c]Melt pond water depth was 0.3 (Table S1).

[d]Melt pond water depth was 0.5–1.2 over the sampling period (Table S1).

lead sites by Nomura et al., 2023). The decision was made to focus additional melt pond analyses specifically on two melt ponds: Stations 1 and 4. Station 1 was a closed pond, and Station 4 was an open pond (Lee et al., 2012). The thickness of the ice below the bottom of the melt pond was measured (0.7 m at Station 4 on September 14 and 1.3 m at Station 1 on September 18) by coring over the refrozen melt pond surface ice after vertical water sampling. In the initial survey, we also included a lead site, which we refer to as the ROV lead site, and a melt pond near the ice-coring site (**Table 1**; Nicolaus et al., 2022). All melt pond and lead stations are shown in **Figure 1**. An overview of activities for melt pond and lead observations are summarized in Table S1.

2.2. Hydrographic observations and water sampling

On August 22, the first day of observations, water was sampled from a depth of 0.3 m in 12 different melt ponds to determine the horizontal distribution of water temperature, salinity, DIC, and TA across the melt ponds. Vertical temperature and salinity profiles were then obtained at Station 4 and the ROV lead site with a RINKO profiler (model ASTD103, JFE Advantech, Japan; Nomura et al., 2022; 2023; 2024c). The uncertainty of the temperature and salinity is ±0.01°C and ±0.01, respectively. Salinity was treated as practical salinity in our study. When the surface was frozen, a 0.15 m × 0.15 m hole was cut with

a hand saw 0.5 m away from the thick sea-ice (1.6 m) margin of the melt pond or lead by using a 2 m pole. The thickness of the melt pond surface ice was measured before the RINKO profiler was lowered into the hole. To avoid disrupting the configuration of the melt pond layers, the RINKO profiler was gently and slowly hand-lowered with a rope until the profiler reached the bottom of the pond. The downcast data were used because the structure of the meltwater layer was disturbed when the RINKO profiler was recovered during the upcast. The thickness of the meltwater layer in each profile was defined as the depth where the density gradient was steepest in the depth profile and exceeded 0.1 kg m^{-3} cm^{-1} (Nomura et al., 2023).

After the initial survey of melt ponds, a long-term thermistor probe (TR-5120, T&D Corp., Nagano, Japan) was installed at Station 1 for the duration of Leg 5 to monitor temperatures at water depths of 0.015 m, 0.05 m, 0.1 m, and 0.2 m. The temperature data were stored in a data logger (TR-52i, T&D Corp.; Nomura et al., 2024d). Station 1 was chosen for this installation due to the small size of the melt pond (**Table 1**), which allowed for the suspension of the thermistor in the center of the pond from a pole laid across the pond margins. No further sampling was undertaken at Station 1 to avoid disturbing the measurements from the probe.

Prior to collecting water samples from Station 4 and the ROV lead site to make further measurements, we

checked the vertical structure and depth of the meltwater layers from the same hole used for the RINKO profiler by attaching a conductivity sensor (Cond 315i, WTW GmbH, Germany) to the lower end of a 2-m-long ruler and inserting it into the melt pond and lead waters until the salinity measured with the Cond 315i increased at the interface between meltwater and seawater (halocline) to decide the depth for water sampling. Using tubing attached alongside the sensor, water was pumped up with a peristaltic pump equipped with PTFE tubbing (L/S Pump Tubing, Masterflex, USA) at depths corresponding to meltwater (surface), halocline, and seawater (bottom), with continuous salinity measurements via the conductivity sensor. The collected seawater was subsampled for measurements of dissolved inorganic carbon (DIC), total alkalinity (TA), and the seawater oxygen isotope composition ($\delta^{18}O$; Nomura et al., 2024b). Immediately after subsampling for measurement of DIC and TA, a 6.0% (by wt.) mercuric chloride ($HgCl_2$) solution (100 μL) was added to stop biological activity. All samples were stored at 4°C on the R/V *Polarstern*.

During the discrete water sampling at Station 4 and the ROV lead site, the CO_2 concentration in the water column was measured directly on site at each depth (i.e., surface, halocline, and bottom) by passing the water from the peristaltic pump through an equilibrator Liqui-Cel® (G542, S/N: 132462, 3M Company, USA) connected to an infrared gas analyzer (LI-8100A, LI-COR Inc., USA; Nomura et al., 2024b). The analyzer was calibrated with standard gases containing 0.0, 299.3, and 501.3 ppm CO_2 before the expedition. Root means square (RMS) noise at 370 ppm with 1-second signal averaging is <1 ppm (https://www.licor.com/env/products/soil-flux/LI-8100a). The sample was passed through the equilibrator for about 1 minute prior to analysis to allow CO_2 to equilibrate with air. At Station 4 and the ROV lead site, vertical CO_2 measurements were made every 0.05 m to obtain detailed profiles. The pCO_2 (μatm) was calculated from the CO_2 concentration (ppm) in the air equilibrated with water, the barometric pressure, and the saturated water vapor pressure (Weiss and Price, 1980).

2.3. CO₂ flux between the atmosphere and the surface of ice and water by chambers

We measured the CO_2 fluxes between the atmosphere and the surface of the melt pond or the lead, sea ice, and snow (Nomura et al., 2024a) at Station 4, the ROV lead site, and the ice-coring site. When the surface of the melt pond or lead was frozen, flux measurements were made over the frozen surface for 1−2 hours. Then, a 1 m × 1 m hole was cut with a hand saw, and chambers were installed over the water surface with buoyant material (Nomura et al., 2020; 2022).

We used LI-COR 8100−104 chambers connected to a LI-8100A soil CO_2 flux system (LI-COR Inc., USA) to measure the fluxes. A chamber was connected via a closed loop to an infrared gas analyzer (LI-8100A, LI-COR Inc., USA) to measure CO_2 concentrations with an air pump at a rate of 3 L minute^{-1} during 20-minute intervals. Power was supplied by a battery (8012−254, Optima Batteries Inc., USA).

We also used a Teflon-coated metal chamber (0.50 m in diameter and 0.30 m high with a serrated bottom edge; Nomura et al., 2010; 2012). Every 5−10 minutes during an experiment (20 minutes), about 500 mL of air was collected from the chamber using a 50 mL glass syringe with a 3-way valve and then transferred to a 3000-mL Tedlar bag (AAK 3L, GL Sciences Inc., Japan). To avoid any effect from pressure changes during the collection of air samples, a 3000 mL Tedlar bag was installed within the chamber as a pressure regulator. After collection, air samples were quickly transported in a dark container to a laboratory onboard the R/V *Polarstern*. The CO_2 concentrations were measured with a CO_2 analyzer (Picarro 2132-i) used for continuous measurements of atmospheric CO_2/CH_4 concentrations on board.

The CO_2 fluxes (in mmol m^{-2} day^{-1}; a negative value indicates CO_2 being absorbed from the atmosphere) were calculated based on the changes in the CO_2 concentrations within the headspace of the chambers. The detection limit of the system is about +0.1 mmol m^{-2} day^{-1} (Nomura et al., 2010; 2018b). An inter-comparison experiment between the metal chamber and the LI-COR 8100−104 chamber in the home laboratory indicated good agreement (Nomura et al., 2022). Data obtained with both methods were therefore considered comparable.

Atmospheric CO_2 concentrations were measured in a Swiss container onboard the R/V *Polarstern* (Angot et al., 2022). Atmospheric pCO_2 was calculated from the observed CO_2 concentration, air temperature, and air pressure during MOSAiC Leg 5 (Schmithüsen et al., 2021).

2.4. Artificial mixing experiments in the melt pond and lead

We conducted water mixing experiments at Station 4 on September 2 and at the ROV lead site on September 5 to understand how the carbonate chemistry and CO_2 fluxes in the melt pond and lead responded to changes in the marine environment caused by wind and movement of sea ice. Before the mixing experiments, we measured the salinity and CO_2 concentrations at depths of 0.05 m in the melt pond and 0.1 m in the lead with an equilibrator, and concomitantly measured the sea–air fluxes using the metal chamber adapted to float on the water surface. The water in the melt pond or lead was then mixed vigorously for 30 minutes by two persons using canoe paddles. After mixing, further water column and surface flux measurements were taken.

2.5. Sample analysis

Oxygen isotope analyses were carried out with a mass spectrometer (DELTA-S Finnigan MAT, USA) at the ISOLAB Facility of the Alfred Wegener Institute in Potsdam, Germany, using the equilibration method (details in Meyer et al., 2000; 2022). The $\delta^{18}O$ values in per mil (‰) were calculated using the $^{18}O/^{16}O$ ratio of Vienna standard mean ocean water (V-SMOW) as the standard. The standard deviation of $\delta^{18}O$, calculated from six subsamples of the reference water ($\delta^{18}O = -0.07$‰), was <0.05‰.

The DIC of seawater was determined by coulometry (Johnson et al., 1985; Johnson, 1992) using a home-made

CO_2 extraction system (Ono et al., 1998) and a coulometer (CM5012, UIC, Inc., Binghamton, NY, USA). The TA of seawater was determined by titration (Dickson et al., 2007) using a TA analyzer (ATT-05, Kimoto Electric Co., Ltd., Japan). Both DIC and TA measurements were calibrated with reference seawater samples (Batch AR, AU, and AV; KANSO Technos Co., Ltd., Osaka, Japan; https://www.kanso.co.jp/eng/) traceable to the Certified Reference Material distributed by Prof. A. G. Dickson (Scripps Institution of Oceanography, La Jolla, CA, USA). The standard deviations of the DIC and TA measurements, calculated from 10 subsamples taken from reference water with a DIC value of 2039.4 μmol kg^{-1} and a TA value of 2311.6 μmol kg^{-1}, were $\pm$1.4 μmol kg^{-1} and $\pm$1.2 μmol kg^{-1}, respectively. The pCO$_2$ was calculated from the DIC and TA using CO2SYS ver. 02.05 (Orr et al., 2018). We used the carbonic acid dissociation constants (K1 and K2) of Goyet and Poisson (1989). The KHSO$_4$ was determined as described in Dickson (1990). We estimated the error on the pCO$_2$ to be less than 6.0% by calculating the effect of changing the DIC and TA values by their standard deviation of the DIC and TA measurements.

2.6. Fractions of snow and sea-ice meltwater and under-ice seawater

To identify the origin of the meltwater within a melt pond or lead, we estimated the fractions of snow meltwater, sea-ice meltwater, and seawater with the following equations (Østlund and Hut, 1984):

$$F_{snow} + F_{si} + F_{sw} = 1 \qquad (1)$$

$$F_{snow}\, S_{snow} + F_{si}\, S_{si} + F_{sw}\, S_{sw} = S_{obs} \qquad (2)$$

$$F_{snow}\, \delta_{snow} + F_{si}\, \delta_{si} + F_{sw}\, \delta_{sw} = \delta_{obs} \qquad (3)$$

where F, S, and δ represent the fraction, salinity, and $\delta^{18}O$, respectively. The subscripts "snow", "si", "sw", and "obs" refer to snow meltwater, sea-ice meltwater, seawater, and the observed (measured) values in water, respectively. The fractions obtained with Equations (1)–(3) are expressed as percentages in the following text. The end-member values for snow and sea ice were taken from Leg 4, as in Nomura et al. (2023), which might have contributed to the Leg 5 melt ponds (Lange et al., 2023). For seawater, values sampled on August 22 from a depth of 10 m were used. The end-member values for snow, sea ice, and seawater are shown in **Table 2**. According to Nomura et al. (2023), taking the standard

Table 2. Mean end-member values ($\pm$standard deviation) for snow meltwater, sea-ice meltwater, and seawater

Sample	Salinity	$\delta^{18}O$ (‰)	N values
Snow meltwater[a]	0	-19.1 ± 9.8	67
Sea-ice meltwater[a]	2.4 ± 0.3	-0.39 ± 0.47	21
Seawater[b]	32.6	-1.25	1

[a]Samples were collected during Leg 4 (Lange et al., 2023).

[b]From 10 m depth on August 22.

deviations of salinity and $\delta^{18}O$ measurements into account, the three fractions varied maximally by 1.9%.

3. Results

3.1. Vertical profiles of temperature, salinity, density, DIC, TA, and pCO$_2$

At Station 4, the vertical profiles of temperature, salinity, and density were obtained from the surface of the melt ponds to a depth of about 1.2 m (**Figure 2**). In the top 0.6 m, the three parameters remained largely consistent around $-1.5°C$ (temperature), 28 (salinity), and 1022 kg m^{-3} (density) between August 28 and September 8. In contrast, in the bottom 0.6 m depth, temperature successively decreased from a maximum of about 0.2°C at the end of August to $-1.5°C$ in mid-September. At the same time, the salinity increased from 0.3 to 28, and the density from 1000 to 1022 kg m^{-3}.

The vertical distributions of salinity, DIC, and TA from water samples at Station 4 were very similar on August 28, September 2, and September 14 (**Figure 3**). All values were lowest in the surface layer and increased with depth. Furthermore, salinity, DIC, and TA increased with time in the surface and halocline. In contrast, there was little temporal change in the bottom layer.

Surface pCO$_2$ at Station 4 on August 28 and September 2 ranged from 364 μatm to 385 μatm and was undersaturated compared to the atmosphere (**Figure 3d**). Values in the bottom layer ranged from 286 μatm to 303 μatm. On August 28 and September 2, pCO$_2$ was lower in the halocline, from 155 μatm to 166 μatm. However, on September 14, when the salinity of the melt pond water at both sampling depths was similar to that of seawater, the pCO$_2$ values were close to 300 μatm.

At the ROV lead site, on September 4 and 5, the pCO$_2$ was again undersaturated in the surface layer (328–364 μatm) compared to the atmosphere (**Figure 4**). Inside the lead, as in the melt pond, there was a pattern of meltwater layer–halocline–seawater layer, with the pCO$_2$ clearly lowest in the halocline (79–154 μatm). From September 4 to September 5, the meltwater layer thinned, and the halocline moved closer to the lead surface. At the same time, low-pCO$_2$ seawater moved to the surface. Below the halocline, pCO$_2$ was vertically uniform, as was salinity.

3.2. Spatial distribution of the carbonate species in the melt pond

At the beginning of the observations on August 22, DIC and TA were analyzed at 12 melt ponds alongside water temperature and salinity (**Table 1**). The water temperature was 0.0 to 0.6°C and salinity was 0.2 to 2.3. The pCO$_2$ calculated from the DIC and TA varied from 138 to 386 μatm, which was undersaturated compared to the atmosphere (400 $\pm$ 3 μatm).

3.3. Temporal variations of air and water temperatures, wind speed, and thickness of the meltwater layer

After an initial phase of air and water temperatures around 0°C from late August until September 4, the air temperatures dropped to below $-10°C$, and the water
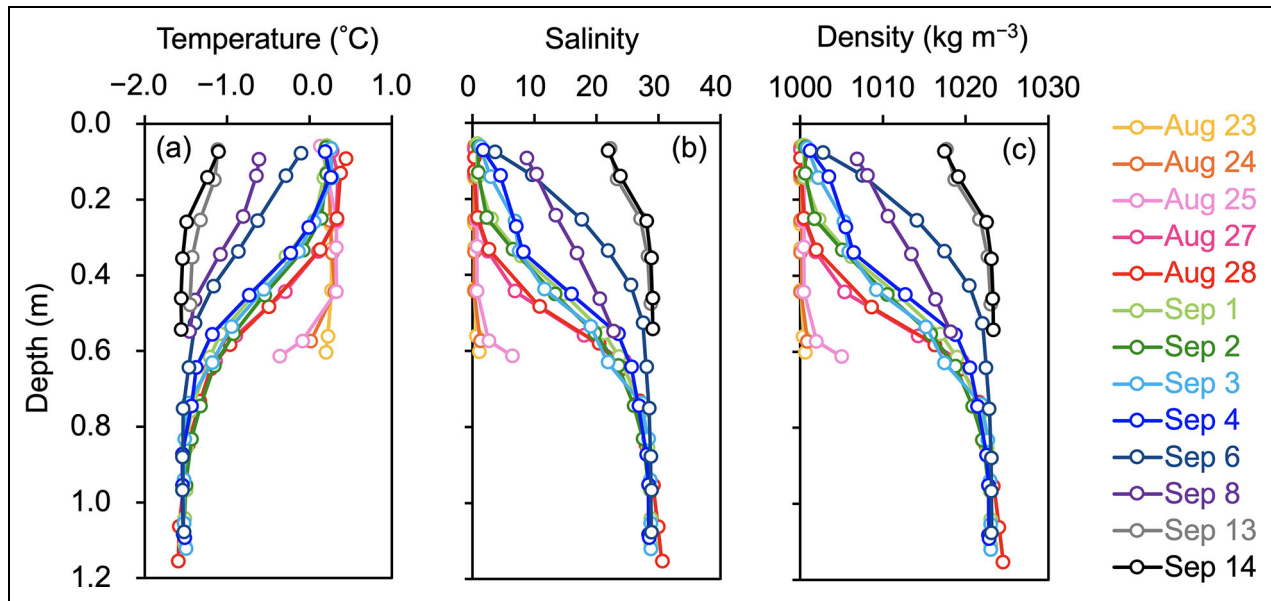
Figure 2. Temporal changes in melt pond water mass characteristics over the MOSAiC Leg 5 sampling period. Results from CTD casts at melt pond Station 4 obtained between August 23 and September 14, 2020. Panels (a), (b), and (c) depict depth profiles of water temperature (°C), salinity, and density (kg m^{-3}), respectively, over 0.1 m depth intervals.
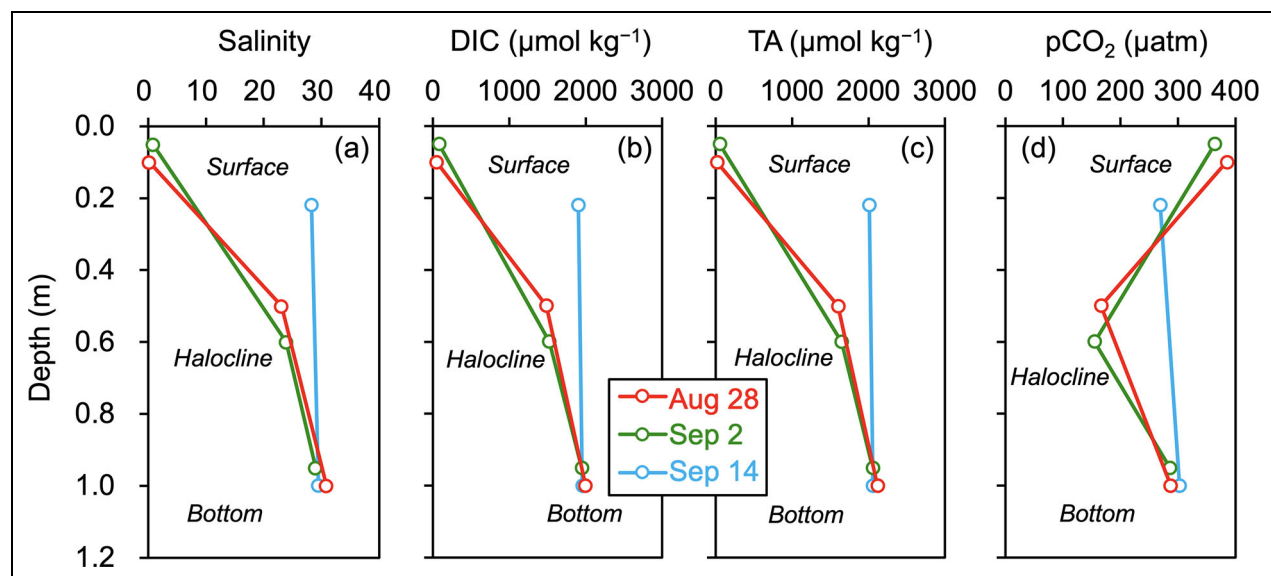
Figure 3. Temporal changes in carbonate chemistry. (a) Salinity, (b) DIC (μmol kg^{-1}), and (c) TA (μmol kg^{-1}) determined on melt pond water samples collected at Station 4. Panel (d) shows the vertical profile of pCO$_2$ calculated from these results using CO2SYS. Red, green, and blue indicate the results for August 28, September 2, and September 14, 2020, respectively.

temperature at Station 1 decreased to about −1.5°C (**Figure 5a** and **c**). The melt water layer at Station 4 successively shrunk from 0.6 m until it completely vanished by September 13 (**Figure 5d**). Wind speeds varied from 1 m second^{-1} to 15 m second^{-1}, averaging approximately 7 m second^{-1} over the observation period. Storm events with wind speeds exceeding 12 m second^{-1} were observed on September 7 and September 14 (**Figure 5b**).

3.4. Fractions of under-ice seawater, sea-ice meltwater, and snow in the melt pond

Based on discrete water sampling at Station 4 on September 2, salinity was low in the surface layer (0.8 at 0.05 m) and increased with depth, as observed in the RINKO salinity profiles (**Figure 2b**). At the bottom (0.95 m) of the melt pond the salinity (29.0) was of similar order as the salinity of the seawater measured at 10 m below the sea ice (32.6) on August 22 (Nomura et al., 2023; **Table 2**).
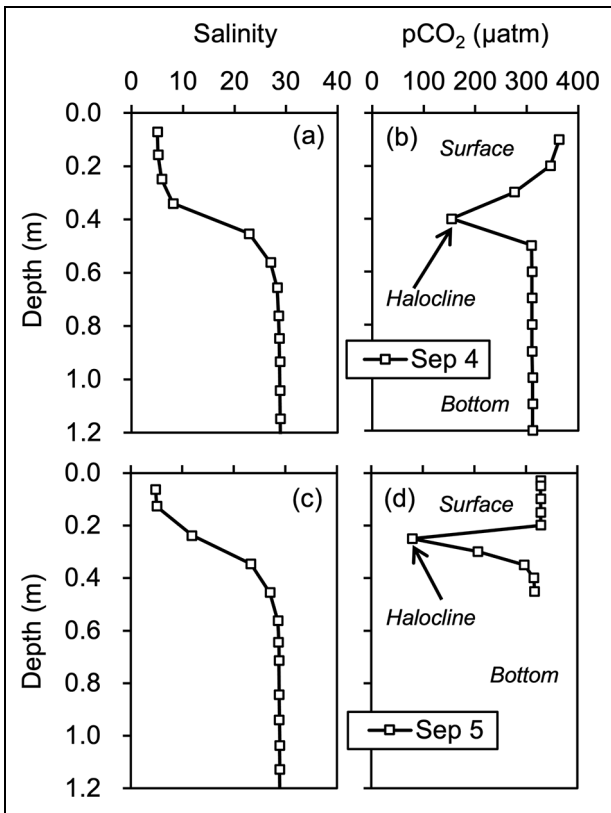
Figure 4. Vertical profiles of salinity and pCO_2. (a) Salinity measured at the ROV lead site using a RINKO profiler and (b) CO_2 concentrations measured using an equilibrator, converted to pCO_2 for the result on September 4. (c) and (b) are the results on September 5 for salinity and CO_2 concentrations, respectively. Plots indicated by arrows in (b) and (d) show the pCO_2 at the halocline.

The $\delta^{18}O$ was higher in the halocline ($-1.64‰$ at 0.6 m) than in the surface and bottom layers (**Table 3**).

The water sampled from the surface (0.05 m) consisted of 89% sea-ice meltwater and 11% snow meltwater (with no seawater present). As depth increased, the fraction of sea-ice meltwater decreased, and conversely, the fraction of seawater increased. In the halocline (0.06 m) and bottom (0.95 m) of the melt pond, seawater accounted for 70% and 89% of the water, respectively. The fraction of snow meltwater ranged from 4% to 11% from the surface to the bottom layer (**Table 3**).

3.5. CO_2 flux between the atmosphere and the surface of ice and water by chambers

On both August 31 and September 7, the fluxes over the sea ice near the melt pond were slightly positive (0.4 ± 0.3 mmol m^{-2} day^{-1} on August 31, 0.6 ± 0.2 mmol m^{-2} day^{-1} on September 7). In contrast, the fluxes between the atmosphere and the melt pond surface were negative on both days (-0.7 ± 0.3 mmol m^{-2} day^{-1} on August 31, -1.0 ± 0.7 mmol m^{-2} day^{-1} on September 7). In other words, CO_2 is released from the sea ice and absorbed by the melt pond surface. The CO_2 flux from the frozen melt pond to the atmosphere was 0.1 ± 0.04 mmol m^{-2} day^{-1} (**Table 4**).
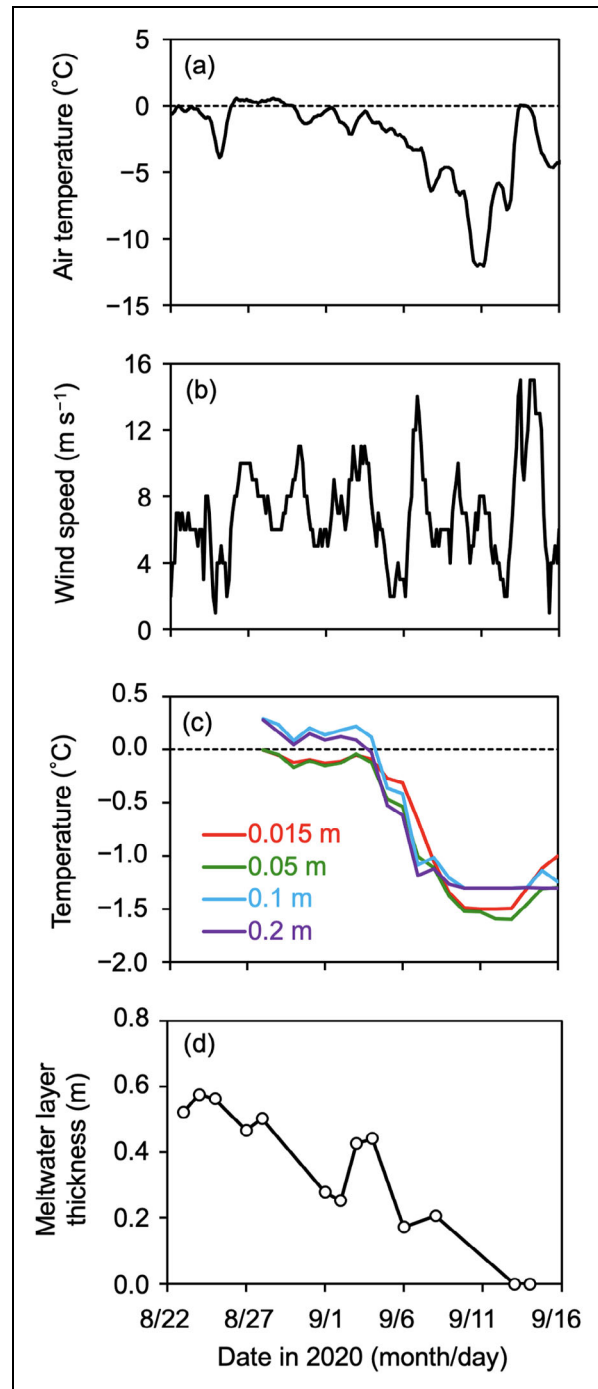

Figure 5. Temporal changes in air temperature, wind speed, and melt pond stratification. Temporal variations of (a) 12-hour mean air temperature, (b) 3-hour mean wind speed, (c) daily mean temperature at water depths of 0.015 m, 0.05 m, 0.1 m, and 0.2 m at Station 1 measured by thermistor probe, and (d) meltwater layer thickness at Station 4 during the observation period. (a) and (b) were measured at the 25 m height mast of the R/V *Polarstern* (Schmithüsen et al., 2021). The dashed horizontal lines in (a) and (c) represent 0°C.

3.6. Mixing experiments in melt pond and lead water

The mixing experiment in the melt pond showed an increase in salinity, a decrease in pCO_2, and an increase in CO_2 absorption (**Table 5**). The mixing experiment at the

Table 3. Values for salinity, $\delta^{18}O$ and the fraction of snow (F_{snow}), sea ice (F_{si}), and seawater (F_{sw}) at Station 4 on September 2, 2020

Layer	Salinity	$\delta^{18}O$ (‰)	Fraction (%) F_{snow}	F_{si}	F_{sw}
Surface	0.8	−2.82	12.6	87.4	0.0
Halocline	23.9	−1.64	3.4	25.1	71.5
Bottom	29.0	−3.18	10.8	0.3	88.9

Table 4. Mean CO_2 flux (±standard deviation) for each surface type at the ice-coring site

Date (2020)	Surface Condition	CO_2 Flux (mmol m^{-2} day^{-1})	N Values
Aug 31	Sea ice (no snow)	0.4 ± 0.3	3
	Melt pond water	−0.7 ± 0.3	7
Sep 7	Sea ice (2 cm thick snow)	0.6 ± 0.2	2
	Melt pond water	−1.0 ± 0.7	3
	Melt pond surface ice (5.5 cm thick ice)	0.1 ± 0.04	4

Table 5. Values for salinity, pCO_2, and CO_2 flux before and after the mixing experiments

Melt Pond or Lead	Salinity	pCO_2 (µatm)	CO_2 Flux (mmol m^{-2} day^{-1})
Station 4 before[a]	0.8	321	−3.9
Station 4 after[a]	6.5	81	−21.0
ROV lead site before[b]	4.6	345	−0.5
ROV lead site after[b]	20.0	278	−4.9

[a]September 2.

[b]September 5.

ROV lead site resulted in similar observations as for the melt pond.

4. Discussion

4.1. Temporal variations during melt pond evolution

Based on changes in salinity (**Figure 2b**) and meltwater layer thickness (**Figure 5d**), the melt pond at Station 4 (considered to be an open pond) was initially filled with meltwater (mainly sea-ice meltwater; see Section 3.4). Over time, seawater entered into the pond through the bottom. In the final stages, the meltwater layer thickness in the melt pond began to decrease (**Figure 5d**), and finally the pond was filled with seawater completely

(**Figures 2c** and **3a**). This evolution of melt pond at Station 4 suggests that it was in the transition period from the third stage to the fourth stage. In such melt ponds, the exchange of meltwater and seawater occurs through spot holes at the bottom of melt pond (i.e., cracks, seal holes) and brine channels (Polashenski et al., 2012; Marsay et al., 2018). The aerial image in **Figure 1** reveals holes (dark areas) that were connected to the sea at the bottom of many melt ponds during the observation period, as indicated by the type open in **Table 1**. Lee et al. (2012) reported that surface water (at most within 0.1 m depth) in the open ponds had a higher salinity than closed ponds, with a value close to that of the underlying seawater, and did not mention the stage of the melt pond in their study. Judging from the observation period and the high salinity and unfrozen water in the open pond surface, it can be assumed that these melt ponds they observed were at the third stage. However, both melt ponds investigated in our study, that is, melt ponds at Stations 4 and 1, respectively considered to be open and closed ponds, had low salinities (<2.3; **Table 1**). As indicated in **Figure 2b**, the melt ponds were filled with meltwater or stratified in the early stages of observation showing no difference in surface salinity between open and closed ponds in contrast to the observations of Lee et al. (2012).

Compared to melt pond sampling (Stations 1 and 4), we found a similar progression in salinity changes at the ROV lead site and a nearby lead (Stations 3 and 8; Nomura et al., 2023) compared to the melt ponds. A low-salinity (approximately 5.0) water layer was initially present in the surface layer of the lead, with a sharp change in salinity at a depth of about 1 m, and the salinity was uniform at values of about 32 at depths below 1 m (**Figure 4**). The meltwater layer thickness at the ROV lead site varied from 0.44 m to 0.27 m as time progressed. Nomura et al. (2023) found that the mixing in the lead (Stations 3 and 8) could be explained by wind-induced ice floe drift. There was a strong correlation between wind speed and ice drift speed during MOSAiC Leg 5 ($r^2 = 0.60$, $p < 0.001$; Nomura et al., 2023). The changes in the characteristics of the water in the leads and melt ponds were very similar, suggesting that the water in the melt ponds was mixed with under-ice water through holes at the bottom of the melt pond due to wind-induced ice floe drift. Melt ponds and leads are not independent structures; rather, they interact with each other through holes and cracks in the sea ice. In the melt pond, as in the lead, there was a meltwater layer at the surface, and after a sharp salinity change over time, it appears to be replaced by seawater (**Figure 2b**). Eicken et al. (2002) have reported through tracer experiments that melt ponds are connected to each other and that melt ponds interact through horizontal water exchange and other processes. Smith et al. (2023) have also reported that meltwater exchange can occur within the ice via a complex system of cracks, leads, and melt ponds. The implication is that the changes observed in melt ponds were not a local phenomenon but were likely a widespread occurrence in surrounding cracks and leads.

Table 6. End-member values for salinity, dissolved inorganic carbon (DIC), total alkalinity (TA), pCO₂, and pH for the melt pond Station 4

Date (2020)	Layer	Salinity	DIC (μmol kg^{-1})	TA (μmol kg^{-1})	pCO$_2$ (μatm)[a]	pH[a]
Aug 28	Surface	0.2	47	17	385	6.1
	Bottom	30.9	1996	2114	288	8.1
Sep 2	Surface	0.8	80	52	364	6.6
	Bottom	29.0	1948	2054	286	8.1

[a]Calculated from CO2SYS ver. 02.05 (Orr et al., 2018).

4.2. Effect of mixing melt pond water on carbonate chemistry

Within the melt ponds at Station 4 and the ROV lead site, the pCO$_2$ was lowest in the halocline where meltwater and seawater mixed (**Figures 3d**, **4b**, and **4d**), and the salinity gradient was steepest in the depth profile (**Figures 2b**, **4a**, and **4c**). To investigate the cause of this phenomenon, we examined whether it could be explained by the mixing of meltwater and seawater. We first calculated the variation in pCO$_2$ that would have resulted only from the mixing of meltwater and seawater in the halocline (pCO$_{2\_cal.}$), that is, excluding the effects of biological activity, gas exchange, and precipitation/dissolution of calcium carbonate. The data used in the calculations are from melt pond water on August 28 and September 2, when low-salinity meltwater was present in the surface layer of the melt pond and seawater was present in the bottom layer.

The values of DIC, TA, and salinity in the surface and bottom layers were used as end-members to examine how the relationships between DIC and salinity, TA and salinity, and pCO$_2$ and salinity would have changed by mixing of the two end-members (**Table 6**). **Figure 6a** and **b** shows the DIC and TA at different salinities when surface and bottom waters were mixed on August 28 and September 2, respectively. The slope of the TA–salinity relationship is larger than that of the DIC–salinity relationship, but the intercept is smaller. As a result, the difference between DIC and TA changed sign at a salinity of 6–7; the DIC was higher than the TA in the lower salinity range (<6), and the TA was higher in the higher salinity range (>7). From these DIC and TA results, we calculated pCO$_2$ (**Figure 6c**). For surface meltwater (lower salinity), the pCO$_2$ was about 360 μatm and hence lower than the atmospheric pCO$_2$ (400 $\pm$ 3 μatm). For the bottom seawater (higher salinity), the pCO$_2$ was about 300 μatm. The pCO$_2$ decreased to about 120 μatm when meltwater and seawater were mixed at the halocline, and it reached a minimum at a salinity of about 8 (**Figure 6c**).

Meire et al. (2015) have discussed the low pCO$_2$ of surface waters in Godthåbsfjord, Southwest Greenland: salinity, DIC, and TA behaved conservatively during mixing, in contrast with pCO$_2$ which exhibited a marked non-linear behavior. Indeed, in Godthåbsfjord, when two water masses (one being glacial meltwater with low salinity, DIC, and TA, and the other being high-salinity water in a fjord with high DIC and TA) in equilibrium with the atmosphere were mixed, pCO$_2$ became undersaturated compared to the atmosphere and decreased to 200 μatm at a salinity of about 8. Horikawa et al. (2022) found in Bowdoin Fjord that the pCO$_2$ of surface water decreased when glacial meltwater and seawater were mixed in the fjord and reached a minimum at a salinity of about 12. Although this mixing decreased the pCO$_2$, the decrease in pCO$_2$ was not continuous and reached a minimum around a brackish salinity of 6–12. We also observed a decrease in pCO$_2$ at the halocline of the ROV lead site (**Figure 4b** and **d**). To examine these results in detail, we calculated the mixing ratios of melt pond and lead surface water (i.e., meltwater, with low salinity, DIC, and TA) and pond/lead bottom water (i.e., seawater, with high salinity, DIC, and TA) as end-members with their pCO$_2$ at the time of sampling. The present melt pond study and the lead and fjord survey from Meire et al. (2015) show a similar asymmetric bell-shaped curve (non-linear behavior) that holds true across scales where meltwater mixes with seawater (**Figure 7**). Such a pattern has been reported repeatedly for estuaries (Mook and Koene, 1975; Salisbury et al., 2008; Cai et al., 2013; Abril et al., 2021). The pCO$_2$ is at a minimum at a mixing ratio of around 0.3 (**Figure 7**). We discuss the causes of this pCO$_2$ depression and the non-linearities in carbonate chemistry in detail below.

Figure 8a and **b** shows the pH (seawater scale) and the concentrations of carbonate species (CO_2, HCO_3^-, and CO_3^{2-}) as calculated by CO2SYS in the melt pond on August 28, with the mixing ratio calculated from the end-members. The concentrations of all carbonate species tended to decrease as the mixing ratio decreased from 1.0 (i.e., only seawater) to about 0.3 (i.e., less influence of seawater; **Figure 8b**). Once the mixing ratio became less than 0.3, that is, the influence of meltwater was high, the pH decreased more rapidly (from approximately 8 to 6) compared to higher ratios, leading to strong changes in the carbonate species. The relative abundances of carbonate species in seawater change strongly with pH (**Figure 9**). CO_2 is dominant in the low-pH range, HCO_3^- is dominant near neutral pH, and at higher pH, CO_3^{2-} becomes dominant (Zeebe and Wolf-Gladrow, 2001). Because the pH of seawater (mixing ratio of around 1) is about 8 (**Figure 8a**), HCO_3^- is the dominant carbonate species in seawater (**Figure 8c**). In contrast, the pH of meltwater at the surface of the melt pond (mixing ratio of around 0) was low (6.1; **Figure 8a**). The influence of the meltwater therefore
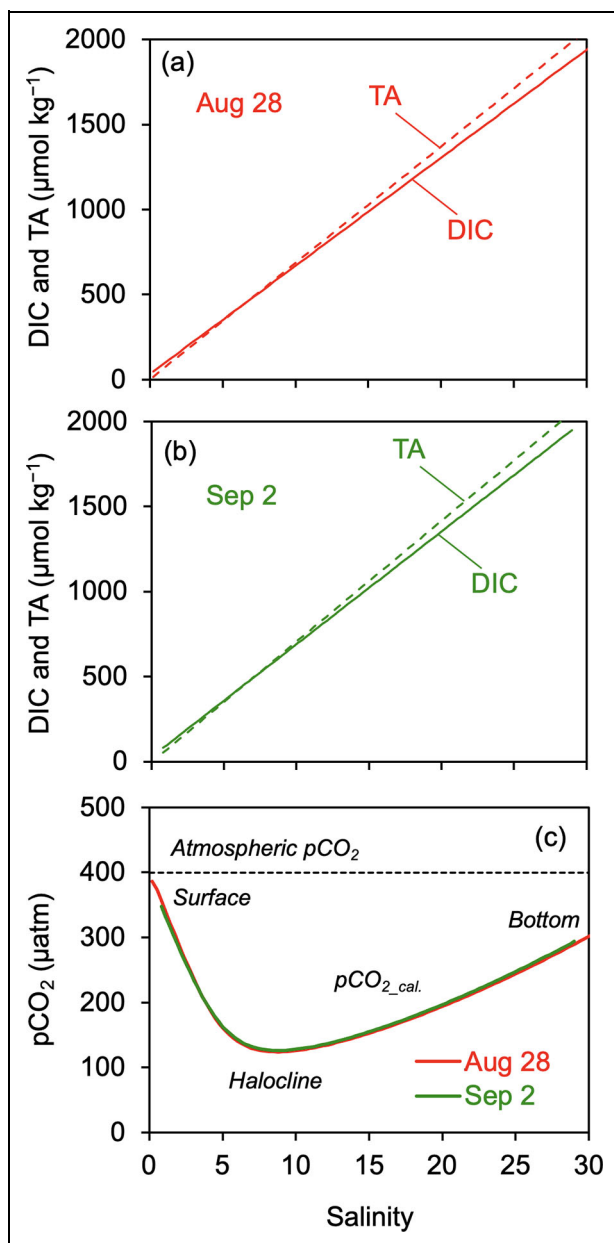
Figure 6. Carbonate chemistry in relation to salinity. DIC (μmol kg^{-1}) or TA (μmol kg^{-1}) of surface and bottom water at Station 4 on August 28 (a) and September 2 of 2020 (b) against salinity, each connected by a straight line. (c) pCO₂ values calculated from DIC and TA for both dates. Atmospheric pCO₂ is the average of values converted from CO₂ concentrations observed in the Swiss container onboard the R/V *Polarstern* during MOSAiC Leg 5 (August 22 to September 14, 2020).

increased near the surface, and the pH decreased rapidly. The result was a larger ratio of CO_2 to CO_3^{2-} in the seawater. As a result, as can be seen from **Figures 6a**, **6b**, **8c**, and **8d**, the DIC in seawater decreased as the salinity (mixing ratio) decreased, but the abundance of CO_2 increased as the mixing ratio decreased to less than about 0.3. The result is a pCO₂ minimum at an intermediate mixing ratio, as shown in **Figure 7**. We applied this analysis to the results of Meire et al. (2015), using as end-members low-salinity water (salinity = 0, DIC = 81 μmol
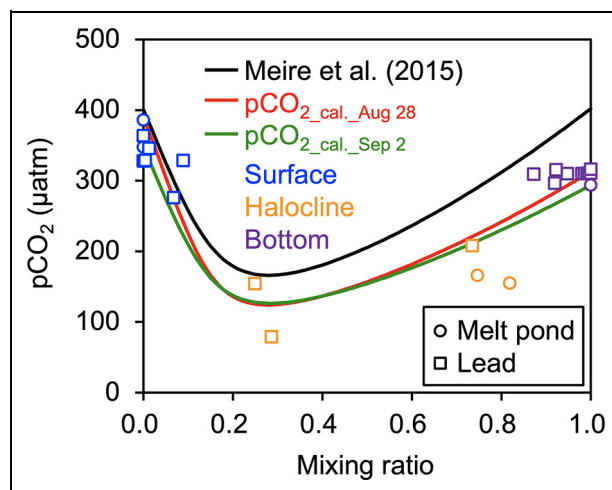

Figure 7. The role of meltwater mixing ratios for pCO₂. The mixing ratio of meltwater in the surface layer and seawater in the bottom layer determined from the salinity (1 for 100% seawater), plotted on the x-axis, and the pCO₂ at that time, plotted on the y-axis.

kg^{-1}, TA = 50 μmol kg^{-1}) and high-salinity water (salinity = 33.65, DIC = 2118 μmol kg^{-1}, TA = 2220 μmol kg^{-1}), with similar results as shown in **Figure 7** and with the trend of pCO₂ variation for different mixing ratios also similar to that in our study. Mook and Koene (1975) have reported non-linear changes of pH and carbonate species due to the mixing of freshwater and seawater in an estuary. According to their calculations, the mixing of seawater and freshwater causes a change of pH, the ratio of carbonate species changes with the change of pH, and the CO_2 increases at low pH. The present calculations for the melt pond halocline are consistent with their results, which also holds true for the computations carried out by Cai et al. (2013) and Abril et al. (2021).

In summary, the change in the pCO₂ profile within the melt pond was determined by physical mixing and non-linearities in carbonate chemistry. The change of pCO₂ due to the mixing of meltwater and seawater in the melt pond decreased the pCO₂ at high salinities by the dilution effect. The pCO₂ reached a minimum where the proportion of meltwater was high and the pH changed significantly (**Figure 8**). Furthermore, the calculations indicate that at lower salinities (i.e., closer to the surface), the pCO₂ approached the atmospheric pCO₂.

4.3. CO₂ exchange with the atmosphere in the melt ponds

The observed CO₂ fluxes between the atmosphere and the surface of the melt pond (Station 4 and ice-coring site), ranged from −3.9 to −0.7 mmol m^{-2} day^{-1}. By convention, negative fluxes correspond to fluxes from the atmosphere to the melt ponds. Semiletov et al. (2004) measured the CO₂ flux between the atmosphere and the melt ponds near Utqiagvik (Barrow), Alaska, in June to range from −51 to −3.9 mmol m^{-2} day^{-1}. Geilfus et al. (2015) also reported CO₂ fluxes in first-year fast ice melt
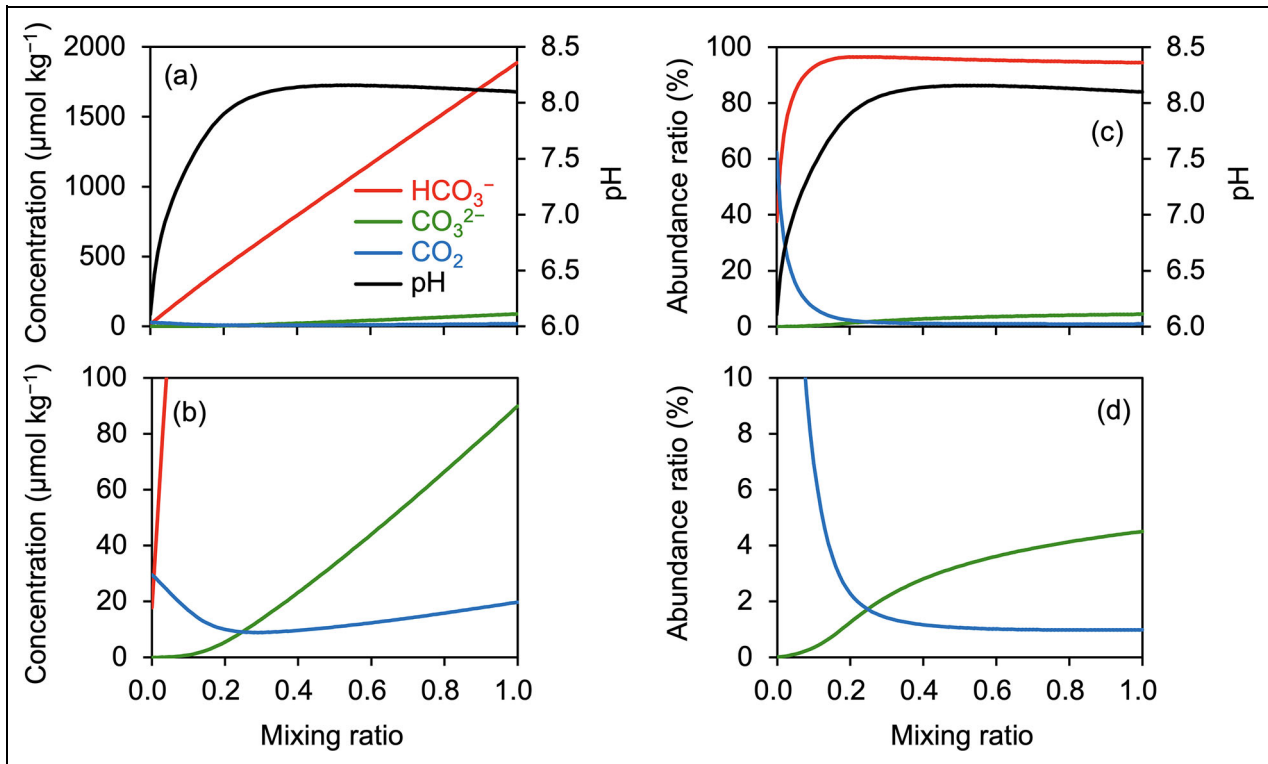
Figure 8. The role of meltwater mixing ratios for carbonate chemistry. (a) The carbonate species (HCO_3^-, CO_3^{2-}, and CO_2) and pH calculated using CO2SYS based on the dissolved inorganic carbon (DIC) and total alkalinity (TA) measurements of the August 28 water sample versus mixing ratio, and (b) an enlarged view of the results for carbonate species. (c) A plot of the abundance ratio of each component when the sum of the three carbonate components in (a) is 100%, and (d) an enlarged view of the plot in (c) for carbonate species.

ponds in Resolute Strait during the spring and summer seasons. According to these authors, melt ponds in the early melting season are formed mainly by snow meltwater, resulting in very low pCO_2 values in the melt ponds (36 µatm, Geilfus et al., 2015). As a result, the atmosphere–melt pond CO_2 fluxes ranged from -5.4 to 0 mmol m^{-2} day^{-1}.

According to Geilfus et al. (2015), melt ponds in the early stages of their evolution continuously absorb CO_2 because their surface water becomes undersaturated compared to the atmospheric CO_2 as a result of meltwater inflow. This condition is the first stage of the melt pond evolution described previously. In contrast, the melt ponds observed in this study were in the third to fourth stage. In these stages, the continuous inflow of meltwater ceases because air temperatures have begun to decrease (Eicken et al., 2004). The pCO_2 in the melt pond surface layer therefore approaches equilibrium with the atmosphere (**Figures 3d** and **6c**), and the uptake of CO_2 decreases, resulting in values lower than those reported by Geilfus et al. (2015) (e.g., -0.7 ± 0.3 mmol m^{-2} day^{-1} on August 31; **Table 4**). The presence of CO_2-near-equilibrated meltwater limited the CO_2 exchange between atmosphere and surface of the melt pond (Smith et al., 2023). The near-equilibrated meltwater layer acts as a cap to the much lower pCO_2 halocline, prohibiting CO_2 exchange between the low pCO_2 water and the atmosphere. As discussed in Section 4.2, when the melt pond was stratified, low-pCO_2 water was present at the halocline (**Figures 3d**, **4b**, and
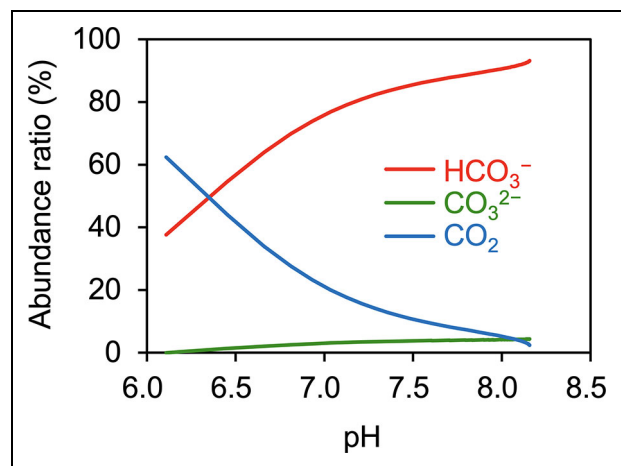

Figure 9. The role of pH for carbonate chemistry. The abundance ratio of carbonate species (HCO_3^-, CO_3^{2-}, and CO_2) versus the pH calculated by CO2SYS.

4d), and this water could continue to absorb CO_2 if it was mixed with the surface meltwater layer. This behavior was apparent in the mixing experiments carried out in our study. Mixing experiments in the melt pond surface layer (0.05 m) resulted in changes of pCO_2 from 321 µatm to 81 µatm, and CO_2 fluxes from -3.9 to -21.0 mmol m^{-2} day^{-1}. These results indicate that significant mixing within stratified melt ponds and leads could reactivate the surface as a significant CO_2 sink from the atmosphere. Natural mixing of melt pond water can occur due to wind
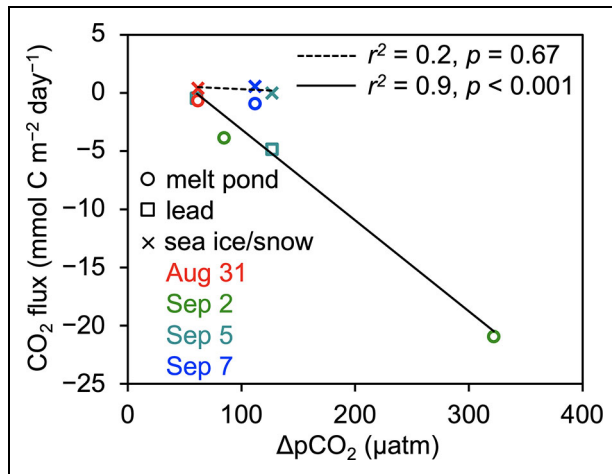
Figure 10. Relationship between CO$_2$ fluxes and ΔpCO$_2$. The difference between pCO$_2$ of surface water at Station 4, ROV lead site and ice-coring site and atmospheric pCO$_2$ (ΔpCO$_2$), versus CO$_2$ fluxes measured by the chamber method between the atmosphere and melt pond/lead water (circle, square) or the atmosphere and ice (cross) at that time. Colors indicate the date (in 2020) of measurement for each sample (red: August 31, ice-coring site; green: September 2, Station 4; light blue: September 5, ROV lead site; blue: September 7, ice-coring site). Solid and dashed lines indicate the linear-fit curve for CO$_2$ fluxes measured over the melt pond/lead water and ice interface, respectively.

mixing and movements of sea ice. Nomura et al. (2023) have documented two storms during the observation period (the first around September 7, and the second around September 13−14), with wind speeds exceeding 12 m second^{-1}. The melt ponds that formed on this Arctic sea ice had the potential to absorb more CO$_2$ from the atmosphere when they were stirred by the wind-induced cooling and the sea ice movement, bringing the low-pCO$_2$ water to the surface layer as shown in the present mixing experiments.

Figure 10 shows the relationship between CO$_2$ fluxes between the atmosphere and the melt pond/lead water surface and difference in pCO$_2$ (ΔpCO$_2$). The fluxes measured at the water surfaces of the melt ponds and the lead decreased with increasing ΔpCO$_2$. In other words, the higher the ΔpCO$_2$ of the melt pond/lead surface layers, the more CO$_2$ was absorbed from the atmosphere. On the other hand, when the surface was frozen and CO$_2$ fluxes were measured over the frozen surface, CO$_2$ absorption from the atmosphere stopped, even if the surface layer of the melt pond was undersaturated compared to the atmosphere (**Figure 10**). Therefore, the CO$_2$ flux measured over the refrozen melt pond ice surface was almost zero (0.1 ± 0.04 mmol m^{-2} day^{-1}; **Figure 10** and **Table 4**). The brine volume fraction, calculated from the temperature (−2.3°C) and bulk salinity (1.3) of the refrozen melt pond ice according to Cox and Weeks (1983), was 2.7%. A brine volume fraction of 5–7.5% or higher is typically taken to indicate that sea ice is permeable to brine

(Golden et al., 1998; Pringle et al., 2009; Zhou et al., 2013). Therefore, the low brine volume fraction calculated for the refrozen melt pond ice surface indicates that no CO$_2$ exchange could occur. Similar results (no gas exchange) were observed for the superimposed ice that formed over Antarctic sea ice and the sea ice in Saroma-ko Lagoon, Hokkaido, Japan, when surface snow was melted and the bottom of the snow refroze (Nomura et al., 2010; 2013; Delille et al., 2014). However, our result showing no CO$_2$ exchange over the refreezing melt pond is the first observation of its kind.

According to the field observations of Webster et al. (2022), melt ponds covered approximately 32% of the MOSAiC Leg 5 sea ice floe. In addition to the melt ponds, cracks and leads were formed in the sea-ice region. The CO$_2$ fluxes measured on the melt ponds and lead in this study indicated CO$_2$ absorption from the atmosphere. Moreover, low pCO$_2$ water was present in the halocline of the melt ponds and lead, and the results of mixing experiments indicated that when the water in the melt ponds and lead was mixed, pCO$_2$ decreased sharply and CO$_2$ absorption increased. Although our study was able to show that changes in pCO$_2$ within a melt pond were determined by physical mixing, respiration, and photosynthesis by organisms living inside the melt pond may have altered the pCO$_2$ to some extent as well. Diatoms and other organisms were observed floating inside the melt pond. Earlier in the season, a unique algal community (halocline flora) was identified at the interface between the meltwater and seawater layers in melt season leads, and the biomass of that algal community remained high for over 4 weeks (Smith et al., 2023). Concentrated algal aggregates were similarly observed in the meltwater layer of leads near the melt pond stations, but at variable states of productivity and decomposition (Smith et al., 2023). Semiletov et al. (2004) have suggested that photosynthesis is accelerated by an increase of photosynthetically active radiation inside a melt pond. However, we were unable to identify significant biogeochemical processes affecting the melt pond pCO$_2$ profile in this summer–autumn time of the year. This observation suggests that there are important CO$_2$ sinks such as melt ponds and leads in the Arctic regions of sea ice, and those sinks can play a role in the overall CO$_2$ budget of the Arctic Ocean, which cannot be ignored when considering the global carbon budget (Steiner et al., 2013).

5. Conclusions

The melt ponds in our survey in the central Arctic Ocean have a lower pCO$_2$ than the atmosphere. CTD observations of the melt ponds indicated that they were initially filled with meltwater, but became stratified over time as seawater intruded from below. The seawater eventually mixed with the meltwater, finally creating a uniform profile in the melt pond. The melt pond disappeared as the surface refroze.

The pCO$_2$ of the water at the interface between the meltwater and underlying seawater is lower than the pCO$_2$ of the meltwater (above) and seawater (below) due to the non-linearities in carbonate chemistry that is changed by the mixing of meltwater and seawater. This decrease in

pCO_2 has been documented in previous studies and was apparent from the direct flux measurements using the chamber method in this study. Experiments we conducted in the field showed that mixing of the meltwater and underlying seawater due to wind or sea-ice turbulence could drive a further drawdown of atmospheric pCO_2. This effect has been observed in leads but also in estuarine systems where freshwater from rivers is mixed with seawater. It appears from the present work to be commonly observed at the surface of sea ice, both in melt ponds and in leads between ice floes.

According to the observations, but also theoretical carbonate system thermodynamics, we suggest that the whole Arctic sea-ice area (both melt pond and lead water) is experiencing this atmospheric pCO_2 drawdown at the surface of melt ponds and leads. A minimum in pCO_2 is observed below the meltwater layer, where we estimate that the mixing ratio between meltwater and seawater is 0.3. This low pCO_2 mixing water is not in contact with the atmosphere. If this low-pCO_2 water is brought to the surface as a result of enhanced mixing, like wind-driven mixing of ice motion, the surface layer pCO_2 would decrease further. By the end of the survey, the pCO_2 in the melt pond surface layer was about the same as that of the seawater under the sea ice and could potentially continue to absorb CO_2 from the atmosphere, but the CO_2 flux became nearly zero as the surface of the melt pond froze. Overall, melt ponds in the Arctic sea-ice area act as moderate sinks for atmospheric CO_2.

Data accessibility statement
The data analyzed in this study were retrieved from links below: RINKO profiler-derived variables: https://doi.pangaea.de/10.1594/PANGAEA.966749, thermistor probe derived variables: https://doi.pangaea.de/10.1594/PANGAEA.966770, water sampler derived variables: https://doi.pangaea.de/10.1594/PANGAEA.966787, CO_2 chamber-derived variables: https://doi.pangaea.de/10.1594/PANGAEA.966833, and meteorological variables: https://doi.org/10.1594/PANGAEA.935267.

Supplemental material
The supplemental files for this article can be found as follows:

Table S1. Overview of activities for melt ponds and leads during the observations. PDF

Competing interests
The authors declare that they have no conflict of interest.

Author contributions
Contributed to conception and design: MY, DN, ALW, MD, ESD, EJC, KMP, HA, BB, BD.
Contributed to acquisition of data: MY, DN, ALW, YL, MD, KS, ESD, EJC, KMP, HA, BB, HM.
Contributed to analysis and interpretation of data: MY, DN, ALW, ESD, MH, MT, BD.
Drafted and/or revised the article: MY drafted the first version of the manuscript, and all authors contributed to writing and revisions.
Approved the submitted version for publication: All authors.

References
Abril, G, **Libardoni, BG**, **Brandini, N**, **Cotovicz, LC Jr**, **Medeiros, PRP**, **Cavalcante, GH**, **Knoppers, BA.** 2021. Thermodynamic uptake of atmospheric CO_2 in the oligotrophic and semiarid Sao Francisco estuary (NE Brazil). *Marine Chemistry* **233**. DOI: https://doi.org/10.1016/j.marchem.2021.103983.

Angot, H, **Beck, I**, **Jokinen, T**, **Laurila, T**, **Quéléver, L**, **Schmale, J.** 2022. Carbon dioxide dry air mole fractions measured in the Swiss container during MOSAiC 2019/2020 [dataset]. PANGAEA. DOI: https://doi.org/10.1594/PANGAEA.944248.

Bates, NR, **Garley, R**, **Frey, KE**, **Shake, KL**, **Mathis, JT.** 2014. Sea-ice melt CO_2-carbonate chemistry in the western Arctic Ocean: Meltwater contributions to air-sea CO_2 gas exchange, mixed-layer properties and rates of net community production under sea ice. *Biogeosciences* **11**(23): 6769–6789. DOI: https://doi.org/10.5194/bg-11-6769-2014.

Bates, NR, **Mathis, JT.** 2009. The Arctic Ocean marine carbon cycle: Evaluation of air-sea CO_2 exchanges, ocean acidification impacts and potential feedbacks. *Biogeosciences* **6**(11): 2433–2459. DOI: https://doi.org/10.5194/bg-6-2433-2009.

Bates, NR, **Moran, SB**, **Hansell, DA**, **Mathis, JT.** 2006. An increasing CO_2 sink in the Arctic Ocean due to sea-ice loss. *Geophysical Research Letters* **33**(23). DOI: https://doi.org/10.1029/2006GL027028.

Cai, W-J, **Chen, CTA**, **Borges, AV.** 2013. Carbon dioxide dynamics and fluxes in coastal waters influenced by river plumes, in Bianchi, TS, Allison, MA, Cai, W-J eds., *Biogeochemical dynamics at major river-coastal interfaces: Linkages with global change.* New York, NY: Cambridge University Press. DOI: https://doi.org/10.1017/CBO9781139136853.010.

Cox, GFN, **Weeks, WF.** 1983. Equations for determining the gas and brine volumes in sea-ice samples. *Journal of Glaciology* **29**: 306–316. DOI: https://doi.org/10.3189/S0022143000008364.

Curry, JA, **Schramm, JL**, **Ebert, EE.** 1995. Sea ice-albedo climate feedback mechanism. *Journal of Climate* **8**(2): 240–247. DOI: https://doi.org/10.1175/1520-0442(1995)008<0240:SIACFM>2.0.CO;2.

Delille, B, **Vancoppenolle, M**, **Geilfus, N-X**, **Tilbrook, B**, **Lannuzel, D**, **Schoemann, V**, **Becquevort, S**, **Carnat, G**, **Delille, D**, **Lancelot, C**, **Chou, L**, **Dieckmann, GS**, **Tison, J-L.** 2014. Southern Ocean CO_2 sink: The contribution of the sea ice. *Journal of Geophysical Research-Oceans* **119**: 6340–6355. DOI: https://doi.org/10.1002/2014JC009941.

Dickson, AG. 1990. Standard potential of the reaction: AgCl(s) + $12H_2$(g) = Ag(s) + HCl(aq), and the standard acidity constant of the ion HSO_4^- in synthetic sea water from 273.15 to 318.15 K. *Journal of Chemical Thermodynamics* **22**(2): 113–127. DOI: https://doi.org/10.1016/0021-9614(90)90074-z.

Dickson, AG, **Sabine, CL**, **Christian, JR** eds. 2007. Guide to best practices for ocean CO_2 measurement. North Pacific Marine Science Organization. (PICES Special Publication 3). DOI: https://doi.org/10.25607/OBP-1342.

Eicken, H. 1994. Structure of under-ice melt ponds in the central Arctic and their effect on the sea-ice cover. *Limnology and Oceanography* **39**(3): 682–694. DOI: https://doi.org/10.4319/lo.1994.39.3.0682.

Eicken, H, **Grenfell, TC**, **Perovich, DK**, **Richter-Menge, JA**, **Frey, K.** 2004. Hydraulic controls of summer Arctic pack ice albedo. *Journal of Geophysical Research-Oceans* **109**(C8). DOI: https://doi.org/10.1029/2003JC001989.

Eicken, H, **Krouse, HR**, **Kadko, D**, **Perovich, DK.** 2002. Tracer studies of pathways and rates of meltwater transport through Arctic summer sea ice. *Journal of Geophysical Research-Oceans* **107**(C10). DOI: https://doi.org/10.1029/2000JC000583.

Feng, J, **Zhang, Y**, **Cheng, Q**, **Tsou, JY.** 2022. Pan-Arctic melt pond fraction trend, variability, and contribution to sea ice changes. *Global and Planetary Change* **217**. DOI: https://doi.org/10.1016/j.gloplacha.2022.103932.

Fernández-Méndez, M, **Katlein, C**, **Rabe, B**, **Nicolaus, M**, **Peeken, I**, **Bakker, K**, **Flores, H**, **Boetius, A.** 2015. Photosynthetic production in the central Arctic Ocean during the record sea-ice minimum in 2012. *Biogeosciences* **12**(11): 3525–3549. DOI: https://doi.org/10.5194/bg-12-3525-2015.

Fernández-Méndez, M, **Wenzhöfer, F**, **Peeken, I**, **Sorensen, HL**, **Glud, RN**, **Boetius, A.** 2014. Composition, buoyancy regulation and fate of ice algal aggregates in the central Arctic Ocean. *Plos One* **9**(9). DOI: https://doi.org/10.1371/journal.pone.0107452.

Geilfus, N-X, **Galley, RJ**, **Crabeck, O**, **Papakyriakou, T**, **Landy, J**, **Tison, J-L**, **Rysgaard, S.** 2015. Inorganic carbon dynamics of melt-pond-covered first-year sea ice in the Canadian Arctic. *Biogeosciences* **12**(6): 2047–2061. DOI: https://doi.org/10.5194/bg-12-2047-2015.

Golden, KM, **Ackley, SF**, **Lytle, VI.** 1998. The percolation phase transition in sea ice. *Science* **282**: 2238–2241. DOI: https://doi.org/10.1126/science.282.5397.2238.

Goyet, C, **Poisson, A.** 1989. New determination of carbonic acid dissociation constants in seawater as a function of temperature and salinity. *Deep-Sea Research Part A-Oceanographic Research Papers* **36**(11): 1635–1654. DOI: https://doi.org/10.1016/0198-0149(89)90064-2.

Gradinger, RR, **Meiners, K**, **Plumley, G**, **Zhang, Q**, **Bluhm, BA.** 2005. Abundance and composition of the sea-ice meiofauna in off-shore pack ice of the Beaufort Gyre in summer 2002 and 2003. *Polar Biology* **28**(3): 171–181. DOI: https://doi.org/10.1007/s00300-004-0674-5.

Horikawa, T, **Nomura, D**, **Kanna, N**, **Fukamachi, Y**, **Sugiyama, S.** 2022. Effects of the glacial meltwater supply on carbonate chemistry in Bowdoin Fjord, Northwestern Greenland. *Frontiers in Marine Science* **9**. DOI: https://doi.org/10.3389/fmars.2022.873860.

Johnson, KM. 1992. Single-operator multiparameter metabolic analyzer (SOMMA) for total carbon dioxide (C{sub T}) with coulometric detection. Operator's manual. SOMMA manual 1.0, January 1992. Upton, NY: Brookhaven National Laboratory: 70. DOI: https://doi.org/10.2172/10194787.

Johnson, KM, **King, AE**, **Sieburth, JM.** 1985. Coulometric TCO_2 analyses for marine studies; An introduction. *Marine Chemistry* **16**(1): 61–82. DOI: https://doi.org/10.1016/0304-4203(85)90028-3.

Lange, BA, **Salganik, E**, **Macfarlane, A**, **Schneebeli, M**, **Hoyland, K**, **Gardner, J**, **Müller, O**, **Divine, DV**, **Kohlbach, D**, **Katlein, C**, **Granskog, MA.** 2023. Snowmelt contribution to Arctic first-year ice ridge mass balance and rapid consolidation during summer melt. *Elementa: Science of the Anthropocene* **11**(1). DOI: https://doi.org/10.1525/elementa.2022.00037.

Lee, SH, **Stockwell, DA**, **Joo, H-M**, **Son, YB**, **Kang, C-K**, **Whitledge, TE.** 2012. Phytoplankton production from melting ponds on Arctic sea ice. *Journal of Geophysical Research-Oceans* **117**. DOI: https://doi.org/10.1029/2011JC007717.

Marsay, CM, **Aguilar-Islas, A**, **Fitzsimmons, JN**, **Hatta, M**, **Jensen, LT**, **John, SG**, **Kadko, D**, **Landing, WM**, **Lanning, NT**, **Morton, PL**, **Pasqualini, A**,

Rauschenberg, S, Sherrell, RM, Shiller, AM, Twining, BS, Whitmore, LM, Zhang, RF, Buck, CS. 2018. Dissolved and particulate trace elements in late summer Arctic melt ponds. *Marine Chemistry* **204**: 70–85. DOI: https://doi.org/10.1016/j.marchem.2018.06.002.

Meire, L, Søgaard, DH, Mortensen, J, Meysman, FJR, Soetaert, K, Arendt, KE, Juul-Pedersen, T, Blicher, ME, Rysgaard, S. 2015. Glacial meltwater and primary production are drivers of strong CO_2 uptake in fjord and coastal waters adjacent to the Greenland Ice Sheet. *Biogeosciences* **12**(8): 2347–2363. DOI: https://doi.org/10.5194/bg-12-2347-2015.

Melnikov, IA, Kolosova, EG, Welch, HE, Zhitina, LS. 2002. Sea ice biological communities and nutrient dynamics in the Canada Basin of the Arctic Ocean. *Deep-Sea Research Part I-Oceanographic Research Papers* **49**(9): 1623–1649. DOI: https://doi.org/10.1016/S0967-0637(02)00042-0.

Meyer, H, Mellat, M, Nomura, D, Damm, E, Bauch, D, Weiner, M, Marent, A. 2022. Stable water isotopes and conductivities of a lead case study during Leg 5 of the MOSAiC expedition. PANGAEA. DOI: https://doi.org/10.1594/PANGAEA.945285.

Meyer, H, Schönicke, L, Wand, U, Hubberten, HM, Friedrichsen, H. 2000. Isotope studies of hydrogen and oxygen in ground ice—Experiences with the equilibration technique. *Isotopes in Environmental and Health Studies* **36**(2): 133–149. DOI: https://doi.org/10.1080/10256010008032939.

Mook, WG, Koene, BKS. 1975. Chemistry of dissolved inorganic carbon in estuarine and coastal brackish waters. *Estuarine and Coastal Marine Science* **3**(3): 325–336. DOI: https://doi.org/10.1016/0302-3524(75)90032-8.

National Snow and Ice Data Center. 2024. Sea Ice Index, Version 3. Microsoft Excel workbook (691 KB). Sea_Ice_Index_Daily_Extent_G02135_v3.0. Available at https://noaadata.apps.nsidc.org/NOAA/G02135/seaice_analysis/Sea_Ice_Index_Daily_Extent_G02135_v3.0.xlsx. DOI: https://doi.org/10.7265/N5K072F8.

Nicolaus, M, Perovich, DK, Spreen, G, Granskog, MA, von Albedyll, L, Angelopoulos, M, Anhaus, P, Arndt, S, Belter, HJ, Bessonov, V, Birnbaum, G, Brauchle, J, Calmer, R, Cardellach, E, Cheng, B, Clemens-Sewall, D, Dadic, R, Damm, E, de Boer, G, Demir, O, Dethloff, K, Divine, DV, Fong, AA, Fons, S, Frey, MM, Fuchs, N, Gabarró, C, Gerland, S, Goessling, HF, Gradinger, R, Haapala, J, Haas, C, Hamilton, J, Hannula, H-R, Hendricks, S, Herber, A, Heuzé, C, Hoppmann, M, Hoyland, KV, Huntemann, M, Hutchings, JK, Hwang, BJ, Itkin, P, Jacobi, H-W, Jaggi, M, Jutila, A, Kaleschke, L, Katlein, C, Kolabutin, N, Krampe, D, Kristensen, SS, Krumpen, T, Kurtz, N, Lampert, A, Lange, BA, Lei, R, Light, B, Linhardt, F, Liston, GE, Loose, B, Macfarlane, AR, Mahmud, M, Matero, IO, Maus, S, Morgenstern, A, Naderpour, R, Nandan, V, Niubom, A, Oggier, M, Oppelt, N, Pätzold, F, Perron, C, Petrovsky, T, Pirazzini, R, Polashenski, C, Rabe, B, Raphael, IA, Regnery, J, Rex, M, Ricker, R, Riemann-Campe, K, Rinke, A, Rohde, J, Salganik, E, Scharien, RK, Schiller, M, Schneebeli, M, Semmling, M, Shimanchuk, E, Shupe, MD, Smith, MM, Smolyanitsky, V, Sokolov, V, Stanton, T, Stroeve, J, Thielke, L, Timofeeva, A, Tonboe, RT, Tavri, A, Tsamados, M, Wagner, DN, Watkins, D, Webster, M, Wendisch, M. 2022. Overview of the MOSAiC expedition: Snow and sea ice. *Elementa: Science of the Anthropocene* **10**(1). DOI: https://doi.org/10.1525/elementa.2021.000046.

Nixdorf, U, Dethloff, K, Rex, M, Shupe, M, Sommerfeld, A, Perovich, D, Nicolaus, M, Heuzé, C, Rabe, B, Loose, B, Damm, E, Gradinger, R, Fong, A, Maslowski, W, Rinke, A, Kwok, R, Spreen, G, Wendisch, M, Herber, A, Hirsekorn, M, Mohaupt, V, Frickenhaus, S, Immerz, A, Weiss-Tuider, K, König, B, Mengedoht, D, Regnery, J, Gerchow, P, Ransby, D, Krumpen, T, Morgenstern, A, Haas, C, Kanzow, T, Rack, FR, Saitzev, V, Sokolov, V, Makarov, A, Schwarze, S, Wunderlich, T, Wurr, K, Boetius, A. 2021. MOSAiC extended acknowledgement. Zenodo. DOI: http://doi.org/10.5281/zenodo.5179739.

Nomura, D, Angelopoulos, M, Stephens, M, Zhan, L, D'Angelo, A, Chamberlain, E, Yoshimura, M, Delille, B. 2024a. CO_2 flux measurements by chambers on sea ice during expedition PS122 (MOSAiC Legs 1–5) to the central Arctic in October 2019–September 2020. PANGAEA. DOI: https://doi.pangaea.de/10.1594/PANGAEA.966833.

Nomura, D, Aoki, S, Simizu, D, Iida, T. 2018a. Influence of sea ice crack formation on the spatial distribution of nutrients and microalgae in flooded Antarctic multiyear ice. *Journal of Geophysical Research-Oceans* **123**(2): 939–951. DOI: https://doi.org/10.1002/2017JC012941.

Nomura, D, Granskog, MA, Assmy, P, Simizu, D, Hashida, G. 2013. Arctic and Antarctic sea ice acts as a sink for atmospheric CO_2 during periods of snowmelt and surface flooding. *Journal of Geophysical Research-Oceans* **118**. DOI: https://doi.org/10.1002/2013JC009048.

Nomura, D, Granskog, MA, Fransson, A, Chierici, M, Silyakova, A, Ohshima, KI, Cohen, L, Delille, B, Hudson, SR, Dieckmann, GS. 2018b. CO_2 flux over young and snow-covered Arctic pack ice in winter and spring. *Biogeosciences* **15**: 3331–3343. DOI: https://doi.org/10.5194/bg-15-3331-2018.

Nomura, D, Ikawa, H, Kawaguchi, Y, Kanna, N, Kawakami, T, Nosaka, Y, Umezawa, S, Tozawa, M, Horikawa, T, Sahashi, R, Noshiro, T, Kaba, I, Ozaki, M, Kondo, F, Ono, K, Yabe, IS, Son, EY, Toyoda, T, Kameyama, S, Wang, CQ, Obata, H, Ooki, A, Ueno, H, Kasai, A. 2022. Atmosphere-sea ice-ocean interaction study in Saroma-ko Lagoon, Hokkaido, Japan 2021. *Bulletin of Glaciological Research* **40**: 1–17. DOI: https://doi.org/10.5331/bgr.21R02.

Nomura, D, Kawaguchi, Y, Webb, AL, Li, YH, Dall'osto, M, Schmidt, K, Droste, ES, Chamberlain, EJ, Kolabutin, N, Shimanchuk, E, Hoppmann, M, Gallagher, MR, Meyer, H, Mellat, M, Bauch, D, Gabarró, C, Smith, MM, Inoue, J, Damm, E, Delille, B. 2023. Meltwater layer dynamics in a central Arctic lead: Effects of lead width, re-freezing, and mixing during late summer. *Elementa: Science of the Anthropocene* **11**(1). DOI: https://doi.org/10.1525/elementa.2022.00102.

Nomura, D, Koga, S, Kasamatsu, N, Shinagawa, H, Simizu, D, Wada, M, Fukuchi, M. 2012. Direct measurements of DMS flux from Antarctic fast sea ice to the atmosphere by a chamber technique. *Journal of Geophysical Research-Oceans* **117**. DOI: https://doi.org/10.1029/2010JC006755.

Nomura, D, Li, Y, Droste, ES, Webb, AL, Chamberlain, E, Yoshimura, M, Meyer, H, Delille, B. 2024b. Melt ponds and leads water sampling for biogeochemical parameters during expedition PS122/5 (MOSAiC Leg 5) to the central Arctic in August–September 2020. PANGAEA. DOI: https://doi.pangaea.de/10.1594/PANGAEA.966787.

Nomura, D, Li, Y, Kawaguchi, Y, Yoshimura, M. 2024c. Profiles of temperature, salinity, and density measured by a handheld CTD in melt ponds during expedition PS122/5 (MOSAiC Leg 5) to the central Arctic in August–September 2020. PANGAEA. DOI: https://doi.pangaea.de/10.1594/PANGAEA.966749.

Nomura, D, Li, Y, Yoshimura, M. 2024d. Water and ice temperatures measured by thermistor probe in a melt pond during expedition PS122/5 (MOSAiC Leg 5) to the central Arctic in August–September 2020. PANGAEA. DOI: https://doi.pangaea.de/10.1594/PANGAEA.966770.

Nomura, D, Simizu, D, Shinagawa, H, Oouchida, C, Fukuchi, M. 2011. Biogeochemical properties of water in surface ponds on Antarctic fast ice and their relationship with underlying sea-ice properties. *Journal of Glaciology* **57**(205): 848–856. DOI: https://doi.org/10.3189/002214311798043825.

Nomura, D, Wongpan, P, Toyota, T, Tanikawa, T, Kawaguchi, Y, Ono, T, Ishino, T, Tozawa, M, Tamura, TP, Yabe, IS, Son, EY, Vivier, F, Lourenco, A, Lebrun, M, Nosaka, Y, Hirawake, T, Ooki, A, Aoki, S, Else, B, Fripiat, F, Inoue, J, Vancoppenolle, M. 2020. Saroma-ko Lagoon observations for sea ice physico-chemistry and ecosystems 2019 (SLOPE2019). *Bulletin of Glaciological Research* **38**: 1–12. DOI: https://doi.org/10.5331/bgr.19R02.

Nomura, D, Yoshikawa-Inoue, H, Toyota, T, Shirasawa, K. 2010. Effects of snow, snowmelting and refreezing processes on air–sea-ice CO_2 flux. *Journal of Glaciology* **56**(196): 262–270. DOI: https://doi.org/10.3189/002214310791968548.

Ono, J, Watanabe, M, Komuro, Y, Tatebe, H, Abe, M. 2022. Enhanced Arctic warming amplification revealed in a low-emission scenario. *Communications Earth & Environment* **3**(1). DOI: https://doi.org/10.1038/s43247-022-00354-4.

Ono, T, Watanabe, S, Okuda, K, Fukasawa, M. 1998. Distribution of total carbonate and related properties in the North Pacific along 30°N. *Journal of Geophysical Research-Oceans* **103**(C13): 30873–30883. DOI: https://doi.org/10.1029/1998JC900018.

Orr, JC, Epitalon, J-M, Dickson, AG, Gattuso, J-P. 2018. Routine uncertainty propagation for the marine carbon dioxide system. *Marine Chemistry* **207**: 84–107. DOI: https://doi.org/10.1016/j.marchem.2018.10.006.

Østlund, HG, Hut, G. 1984. Arctic ocean water mass balance from isotope data. *Journal of Geophysical Research-Oceans* **89**(C4): 6373–6381. DOI: https://doi.org/10.1029/JC089iC04p06373.

Perovich, DK, Grenfell, TC, Light, B, Hobbs, PV. 2002. Seasonal evolution of the albedo of multiyear Arctic sea ice. *Journal of Geophysical Research-Oceans* **107**(C10). DOI: https://doi.org/10.1029/2000JC000438.

Petrich, C, Eicken, H, Polashenski, CM, Sturm, M, Harbeck, JP, Perovich, DK, Finnegan, DC. 2012. Snow dunes: A controlling factor of melt pond distribution on Arctic sea ice. *Journal of Geophysical Research-Oceans* **117**. DOI: https://doi.org/10.1029/2012JC008192.

Polashenski, C, Perovich, D, Courville, Z. 2012. The mechanisms of sea ice melt pond formation and evolution. *Journal of Geophysical Research-Oceans* **117**. DOI: https://doi.org/10.1029/2011JC007231.

Polyakov, IV, Walsh, JE, Kwok, R. 2012. Recent changes of Arctic multiyear sea ice coverage and the likely causes. *Bulletin of the American Meteorological Society* **93**(2): 145–151. DOI: https://doi.org/10.1175/BAMS-D-11-00070.1.

Pringle, DJ, Miner, JE, Eicken, H, Golden, KM. 2009. Pore space percolation in sea ice single crystals. *Journal of Geophysical Research-Oceans* **114**: C12017. DOI: https://doi.org/10.1029/2008JC005145.

Rantanen, M, Karpechko, AY, Lipponen, A, Nordling, K, Hyvärinen, O, Ruosteenoja, K, Vihma, T, Laaksonen, A. 2022. The Arctic has warmed nearly four times faster than the globe since 1979. *Communications Earth & Environment* **3**(1). DOI: https://doi.org/10.1038/s43247-022-00498-3.

Richter-Menge, JA, Perovich, DK, Pegau, WS. 2001. Summer ice dynamics during SHEBA and its effect on the ocean heat content. *Annals of Glaciology* **33**: 201–206. DOI: https://doi.org/10.3189/172756401781818176.

Rösel, A, Kaleschke, L. 2011. Comparison of different retrieval techniques for melt ponds on Arctic sea ice from Landsat and MODIS satellite data. *Annals of Glaciology* **52**(57): 185–191. DOI: https://doi.org/10.3189/172756411795931606.

Salisbury, J, Green, M, Hunt, C, Campbell, J. 2008. Coastal acidification by rivers: A threat to shellfish? *EOS* **89**: 513–528. DOI: https://doi.org/10.1029/2008EO500001.

Schmithüsen, H, Raeke, A, Wenzel, J. 2021. Meteorological observations during POLARSTERN cruise PS122/5. Alfred Wegener Institute, Helmholtz Centre for

Polar and Marine Research, Bremerhaven, PANGAEA. DOI: https://doi.org/10.1594/PANGAEA.935267.

Semiletov, I, **Makshtas, A**, **Akasofu, S-I**, **Andreas, EL.** 2004. Atmospheric CO$_2$ balance: The role of Arctic sea ice. *Geophysical Research Letters* **31**(5). DOI: https://doi.org/10.1029/2003GL017996.

Shupe, MD, **Rex, M**, **Blomquist, B**, **Persson, POG**, **Schmale, J**, **Uttal, T**, **Althausen, D**, **Angot, H**, **Archer, S**, **Bariteau, L**, **Beck, I**, **Bilberry, J**, **Bucci, S**, **Buck, C**, **Boyer, M**, **Brasseur, Z**, **Brooks, IM**, **Calmer, R**, **Cassano, J**, **Castro, V**, **Chu, D**, **Costa, D**, **Cox, CJ**, **Creamean, J**, **Crewell, S**, **Dahlke, S**, **Damm, E**, **de Boer, G**, **Deckelmann, H**, **Dethloff, K**, **Dütsch, M**, **Ebell, K**, **Ehrlich, A**, **Ellis, J**, **Engelmann, R**, **Fong, AA**, **Frey, MM**, **Gallagher, MR**, **Ganzeveld, L**, **Gradinger, R**, **Graeser, J**, **Greenamyer, V**, **Griesche, H**, **Griffiths, S**, **Hamilton, J**, **Heinemann, G**, **Helmig, D**, **Herber, A**, **Heuzé, C**, **Hofer, J**, **Houchens, T**, **Howard, D**, **Inoue, J**, **Jacobi, H-W**, **Jaiser, R**, **Jokinen, T**, **Jourdan, O**, **Jozef, G**, **King, W**, **Kirchgaessner, A**, **Klingebiel, M**, **Krassovski, M**, **Krumpen, T**, **Lampert, A**, **Landing, W**, **Laurila, T**, **Lawrence, D**, **Lonardi, M**, **Loose, B**, **Lüpkes, C**, **Maahn, M**, **Macke, A**, **Maslowski, W**, **Marsay, C**, **Maturilli, M**, **Mech, M**, **Morris, S**, **Moser, M**, **Nicolaus, M**, **Ortega, P**, **Osborn, J**, **Pätzold, F**, **Perovich, DK**, **Petäjä, T**, **Pilz, C**, **Pirazzini, R**, **Posman, K**, **Powers, H**, **Pratt, KA**, **Preusser, A**, **Quéléver, L**, **Radenz, M**, **Rabe, B**, **Rinke, A**, **Sachs, T**, **Schulz, A**, **Siebert, H**, **Silva, T**, **Solomon, A**, **Sommerfeld, A**, **Spreen, G**, **Stephens, M**, **Stohl, A**, **Svensson, G**, **Uin, J**, **Viegas, J**, **Voigt, C**, **von der Gathen, P**, **Wehner, B**, **Welker, JM**, **Wendisch, M**, **Werner, M**, **Xie, ZQ**, **Yue, FG.** 2022. Overview of the MOSAiC expedition: Atmosphere. *Elementa: Science of the Anthropocene* **10**(1). DOI: https://doi.org/10.1525/elementa.2021.00060.

Smith, MM, **Angot, H**, **Chamberlain, EJ**, **Droste, ES**, **Karam, S**, **Muilwijk, M**, **Webb, AL**, **Archer, SD**, **Beck, I**, **Blomquist, BW**, **Bowman, J**, **Boyer, M**, **Bozzato, D**, **Chierici, M**, **Creamean, J**, **D'Angelo, A**, **Delille, B**, **Fer, I**, **Fong, AA**, **Fransson, A**, **Fuchs, N**, **Gardner, J**, **Granskog, MA**, **Hoppe, CJM**, **Hoppema, M**, **Hoppmann, M**, **Mock, T**, **Muller, S**, **Muller, O**, **Nicolaus, M**, **Nomura, D**, **Petäjä, T**, **Salganik, E**, **Schmale, J**, **Schmidt, K**, **Schulz, KM**, **Shupe, MD**, **Stefels, J**, **Thielke, L**, **Tippenhauer, S**, **Ulfsbo, A**, **van Leeuwe, M**, **Webster, M**, **Yoshimura, M**, **Zhan, LY.** 2023. Thin and transient meltwater layers and false bottoms in the Arctic sea ice pack—Recent insights on these historically overlooked features. *Elementa: Science of the Anthropocene* **11**(1). DOI: https://doi.org/10.1525/elementa.2023.00025.

Sørensen, HL, **Thamdrup, B**, **Jeppesen, E**, **Rysgaard, S**, **Glud, RN.** 2017. Nutrient availability limits biological production in Arctic sea ice melt ponds. *Polar Biology* **40**(8): 1593–1606. DOI: https://doi.org/10.1007/s00300-017-2082-7.

Steiner, NS, **Lee, WG**, **Christian, JR.** 2013. Enhanced gas fluxes in small sea ice leads and cracks: Effects on CO$_2$ exchange and ocean acidification. *Journal of Geophysical Research-Oceans* **118**: 1195–1205. DOI: http://doi.org/10.1002/jgrc.20100.

Stroeve, JC, **Kattsov, V**, **Barrett, A**, **Serreze, M**, **Pavlova, T**, **Holland, M**, **Meier, WN.** 2012. Trends in Arctic sea ice extent from CMIP5, CMIP3 and observations. *Geophysical Research Letters* **39**. DOI: https://doi.org/10.1029/2012GL052676.

Takahashi, T, **Sutherland, SC**, **Wanninkhof, R**, **Sweeney, C**, **Feely, RA**, **Chipman, DW**, **Hales, B**, **Friederich, G**, **Chavez, F**, **Sabine, C**, **Watson, A**, **Bakker, DCE**, **Schuster, U**, **Metzl, N**, **Yoshikawa-Inoue, H**, **Ishii, M**, **Midorikawa, T**, **Nojiri, Y**, **Körtzinger, A**, **Steinhoff, T**, **Hoppema, M**, **Olafsson, J**, **Arnarson, TS**, **Tilbrook, B**, **Johannessen, T**, **Olsen, A**, **Bellerby, R**, **Wong, CS**, **Delille, B**, **Bates, NR**, **de Baar, HJW.** 2009. Climatological mean and decadal change in surface ocean pCO$_2$, and net sea-air CO$_2$ flux over the global oceans. *Deep-Sea Research Part II-Topical Studies in Oceanography* **56**(8–10): 554–577. DOI: https://doi.org/10.1016/j.dsr2.2008.12.009.

Taylor, P, **Feltham, D.** 2004. A model of melt pond evolution on sea ice. *Journal of Geophysical Research-Oceans* **109**(C12). DOI: https://doi.org/10.1029/2004JC002361.

Webster, MA, **Holland, M**, **Wright, NC**, **Hendricks, S**, **Hutter, N**, **Itkin, P**, **Light, B**, **Linhardt, F**, **Perovich, DK**, **Raphael, IA**, **Smith, MM**, **von Albedyll, L**, **Zhang, JL.** 2022. Spatiotemporal evolution of melt ponds on Arctic sea ice: MOSAiC observations and model results. *Elementa: Science of the Anthropocene* **10**(1). DOI: https://doi.org/10.1525/elementa.2021.000072.

Weiss, RF, **Price, BA.** 1980. Nitrous oxide solubility in water and seawater. *Marine Chemistry* **8**(4): 347–359. DOI: https://doi.org/10.1016/0304-4203(80)90024-9.

Yasunaka, S, **Siswanto, E**, **Olsen, A**, **Hoppema, M**, **Watanabe, E**, **Fransson, A**, **Chierici, M**, **Murata, A**, **Lauvset, SK**, **Wanninkhof, R**, **Takahashi, T**, **Kosugi, N**, **Omar, AM**, **van Heuven, S**, **Mathis, JT.** 2018. Arctic Ocean CO$_2$ uptake: An improved multiyear estimate of the air-sea CO$_2$ flux incorporating chlorophyll *a* concentrations. *Biogeosciences* **15**(6): 1643–1661. DOI: https://doi.org/10.5194/bg-15-1643-2018.

Zeebe, RE, **Wolf-Gladrow, DA.** 2001. CO$_2$ in seawater: Equilibrium, kinetics, isotopes. Amsterdam, the Netherlands: Elsevier. (Elsevier oceanography series; vol. 65).

Zhou, J, **Delille, B**, **Eicken, H**, **Vancoppenolle, M**, **Brabant, F**, **Carnat, G**, **Geilfus, N-X**, **Papakyriakou, T**, **Heinesch, B**, **Tison, J-L.** 2013. Physical and biogeochemical properties in landfast sea ice (Barrow, Alaska): Insights on brine and gas dynamics across seasons. *Journal of Geophysical Research-Oceans* **118**: 3172–3189. DOI: https://doi.org/10.1002/jgrc.20232.

How to cite this article: Yoshimura, M, Nomura, D, Webb, AL, Li, Y, Dall'osto, M, Schmidt, K, Droste, ES, Chamberlain, EJ, Posman, KM, Angot, H, Blomquist, B, Meyer, H, Hoppema, M, Tozawa, M, Inoue, J, Delille, B. 2025. Melt pond CO_2 dynamics and fluxes with the atmosphere in the central Arctic Ocean during the summer-to-autumn transition. *Elementa: Science of the Anthropocene* 13(1). DOI: https://doi.org/10.1525/elementa.2024.00023

Elem Sci Anth is a peer-reviewed open access journal published by University of California Press.

OPEN ACCESS